Check for updates

Coordination compounds of cobalt(II) with carboxylate non-steroidal anti-inflammatory drugs: structure and biological profile†

Spyros Perontsis, Antonios G. Hatzidimitriou and George Psomas [iD] *

Fourteen cobalt(II) complexes with the non-steroidal anti-inflammatory drugs sodium meclofenamate, tolfenamic acid, mefenamic acid, naproxen, sodium diclofenac, and diflunisal were prepared in the presence or absence of a series of nitrogen-donors (namely imidazole, pyridine, 3-aminopyridine, neocuproine, 2,2′-bipyridine, 1,10-phenanthroline and 2,2′-bipyridylamine) as co-ligands and were characterised by spectroscopic and physicochemical techniques. Single-crystal X-ray crystallography was employed to determine the crystal structure of eight complexes. The biological profile of the complexes was investigated regarding their interaction with serum albumins and DNA, and their antioxidant potency. The interaction of the compounds with calf-thymus DNA takes place *via* intercalation. The ability of the complexes to cleave pBR322 plasmid DNA at the concentration of 500 μM is rather low. The complexes demonstrated tight and reversible binding to human and bovine serum albumins and the binding site of bovine serum albumin was also examined. In order to assess the antioxidant activity of the compounds, the *in vitro* scavenging activity towards free radicals, namely 1,1-diphenyl-picrylhydrazyl and 2,2′-azinobis(3-ethylbenzothiazoline-6-sulfonic acid), and their ability to reduce H_2O_2 were studied.

1. Introduction

The importance of transition metal ions in biological systems is well established for many years and many bioinorganic chemists have focused their research studies on the biological activity of metal ions and their compounds.[1] Among these metal ions, cobalt is included as a trace-element essential for life.[2] The main biological role of cobalt is related with vitamin B12; within this context, cobalt is involved in the synthesis of DNA and the metabolism of fatty acids and amino acids.[3] For this reason, cobalt is also involved in nutrition as a supplement of vitamin B12.[4] Additionally, cobalt(II) ions may interact with Z-DNA[5] or cleave DNA[6] and many cobalt complexes of biological interest have been reported[7,8] mainly because of their potential antitumor, antiproliferative,[9,10] antimicrobial,[11,12] antifungal,[13] antiviral[14,15] and antioxidant[16,17] properties.

Non-steroidal anti-inflammatory drugs (NSAIDs) are a large group of medicaments used to treat pain and inflammation resulting from diseases and/or injuries.[18,19] The main mechanism of action of NSAIDs is the inhibition of the cyclooxygenase-mediated production of prostaglandins.[20] Moreover, NSAIDs can act synergetically with antitumor drugs,[21] and exhibit cytotoxic activity against diverse cancer cell lines *via* mechanisms involving free radical scavenging[22] or programmed cell death.[23] Based on characteristic groups, NSAIDs are categorised as anthranilic acids, phenylalkanoic acids, derivatives of salicylic acid, oxicams, furanones and sulfonamides.[19]

The NSAIDs used in the current research are the anthranilic acids mefenamic acid (Hmef), tolfenamic acid (Htolf), and sodium meclofenamate (Na meclf), the phenylalkanoic acids naproxen (Hnap), and sodium diclofenac (Na dicl), and the salicylate derivative diflunisal (H_2difl) (Fig. 1). All of them are common NSAIDs mainly used as analgesic, anti-inflammatory and antipyretic agents in various treatments. Beside the aforementioned general uses as NSAIDs: Hmef has mild side-effects and is also used to treat migraines and pain from dysmenorrhea;[24] Htolf is also used in veterinary;[25] Na meclofenamate is also administered in osteoarthritis and painful musculoskeletal disorders;[26] Hnap is also used to treat rheumatoid arthritis, chronic migraine, osteoarthritis, and kidney stones,[27] and its use results in milder side-effects concerning blood pressure or stomach ulcers than other NSAIDs;[28,29] sodium diclofenac is administered for treating symptoms of rheumatoid arthritis
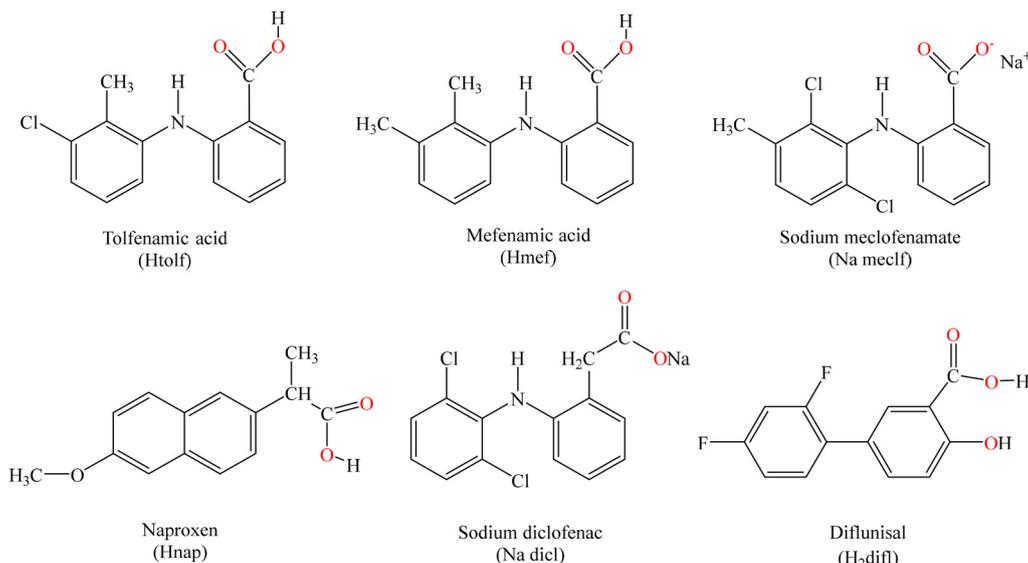
*Department of General and Inorganic Chemistry, Faculty of Chemistry, Aristotle University of Thessaloniki, GR-54124 Thessaloniki, Greece.
E-mail: gepsomas@chem.auth.gr*

†Electronic supplementary information (ESI) available. CCDC 2336775–2336782. For ESI and crystallographic data in CIF or other electronic format see DOI: https://doi.org/10.1039/d4dt01846j

Fig. 1 The syntax formulas of the NSAIDs: tolfenamic acid (Htolf), mefenamic acid (Hmef), sodium meclofenamate (Na meclf), naproxen (Hnap), sodium diclofenac (Na dicl) and diflunisal (H$_2$difl).

and osteoarthritis;[30] diflunisal, because of its relatively long half-life period of activity (~12 h), is used to alleviate acute pain resulting from oral surgery,[31] and has been recently reported to be safely administered to patients suffering from transthyretin amyloidosis cardiomyopathy.[32] Furthermore, most of these NSAIDs were suggested for treatment of the COVID-19 pandemic, regarding their analgetic and antipyretic effects.[33,34] Several reports are found in the literature concerning the synthesis, the characterisation, and the biological evaluation of metal complexes with NSAIDs; a plethora of manganese(II/III),[35–38] iron(III),[39,40] cobalt(II),[16,17,41–46] nickel (II),[47–49] copper(II),[50–53] zinc(II),[54–56] silver(I),[57,58] cadmium(II),[59] tin(IV),[60] gold(I)[61] and lanthanides(III)[62] complexes with the NSAIDs under study have shown enhanced biological properties when compared to the corresponding free NSAIDs.[19,63]

Taken into consideration the enhanced biological profile of metal–NSAID complexes, the significance of NSAID in medication, the biological relevance of cobalt, and as continuation of our research projects concerning Co(II)–NSAID complexes,[16,17,41–43] we have prepared and characterised fourteen cobalt(II) complexes with the NSAIDs Htolf, Hmef, Na meclf, Hnap, Na dicl and H$_2$difl in the presence or absence of N-donors 1H-imidazole (Himi), pyridine (py) and 3-aminopyridine (3-ampy) (Fig. 2(A)) or N,N′-donors 2,9-dimethyl-1,10-phenanthroline (neoc), 2,2′-bipyridine (bipy), 1,10-phenanthroline (phen) and 2,2′-bipyridylamine (bipyam) as co-ligands (Fig. 2 (B)). All resultant complexes **1–14** were characterised by spectroscopic (FT-IR and UV-vis) and physicochemical techniques and the crystal structures of eight complexes were determined by single-crystal X-ray crystallography.

The *in vitro* biological profile of the novel compounds is related with: (i) the antioxidant activity by determining the ability to scavenge free radicals such as 2,2′-azinobis-(3-ethyl-
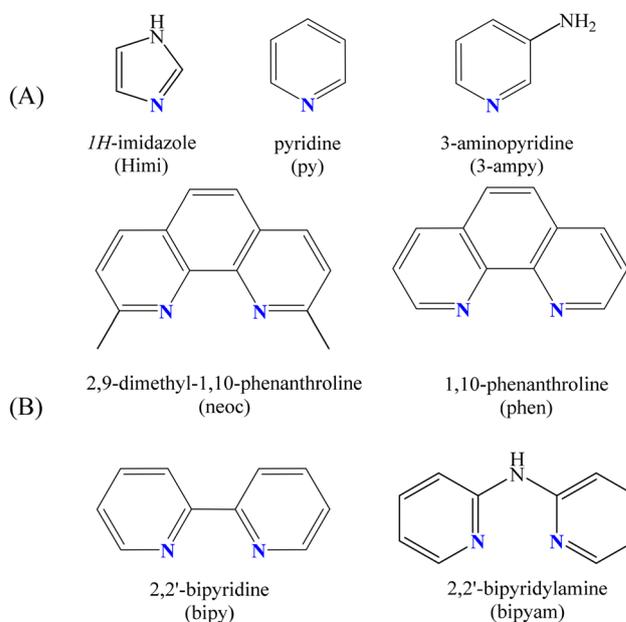
Fig. 2 The syntax formulas of the nitrogen-donor ligands: (A) the N-donor co-ligands: 1H-imidazole (Himi), pyridine (py) and 3-aminopyridine (3-ampy), and (B) the N,N′-donor co-ligands: 2,9-dimethyl-1,10-phenanthroline (neoc), 1,10-phenanthroline (phen), 2,2′-bipyridine (bipy) and 2,2′-bipyridylamine (bipyam).

benzothiazoline-6-sulfonic acid) (ABTS) and 1,1-diphenyl-picrylhydrazyl (DPPH) and to reduce H$_2$O$_2$, (ii) the interaction with calf-thymus (CT) DNA monitored by cyclic voltammetry, viscosity measurements, UV-vis spectroscopy, and *via* competition with the intercalation marker ethidium bromide (EB) by fluorescence emission spectroscopy, (iii) the ability to cleave

supercoiled circular pBR322 plasmid DNA (pDNA) examined by agarose gel electrophoretic experiments, and (iv) the affinity (calculation of binding strength and determination of binding site location) for bovine serum albumin (BSA) and human serum albumin (HSA), investigated by fluorescence emission spectroscopy.

2. Experimental

2.1. Materials–instruments–physical measurements

All chemicals and solvents were of reagent grade and were used as purchased from commercial sources without any further purification. More specifically, $CoCl_2 \cdot 6H_2O$, bipy, bipyam, phen, neoc, Himi, py, 3-ampy, KOH, CT DNA, EB, BSA, HSA, ABTS, $K_2S_2O_8$, nordihydroguaiaretic acid (NDGA), butylated hydroxytoluene (BHT) were purchased from Sigma-Aldrich Co; Na dicl, Htolf, Hmef, Na meclf, Hnap, H_2difl, sodium warfarin, ibuprofen, DPPH from Tokyo Chemical Industry (TCI); 6-hydroxy-2,5,7,8-tetramethylchromane-2-carboxylic acid (trolox) from J&K; trisodium citrate dihydrate, NaCl, NaH_2PO_4 from Merck; supercoiled circular pBR322 plasmid DNA from New England Bioline; Tris base, boric acid, EDTA disodium salt dehydrate, loading buffer and H_2O_2 (30% w/v) from PanReac Applichem; L-ascorbic acid (AA) Na_2HPO_4 and all solvents from Chemlab.

CT DNA stock solution was prepared by the dilution of CT DNA to buffer (containing 15 mM trisodium citrate and 150 mM NaCl at pH 7.0) followed by exhaustive stirring for three days, and was kept at 4 °C for no longer than ten days. The stock solution of CT DNA gave a ratio of UV absorbance at 260 and 280 nm (A_{260}/A_{280}) of 1.87, indicating that the DNA used was sufficiently free of protein contamination.[64] The CT DNA concentration was determined by UV absorbance at 258 nm after 1 : 20 dilution using $\varepsilon = 6600$ M^{-1} cm^{-1}.[65]

Infrared (IR) spectra (400–4000 cm^{-1}) were recorded on a Nicolet FT-IR 6700 spectrometer with samples prepared as KBr disk (abbreviations used: vs = very strong; s = strong; m = medium; $\Delta\nu(COO) = \nu_{asym}(COO) - \nu_{sym}(COO)$). UV-visible (UV-vis) spectra were recorded as nujol mulls and in solution at concentrations in the range 10^{-5}–10^{-3} M on a Hitachi U-2001 dual-beam spectrophotometer. C, H and N elemental analysis was performed on a PerkinElmer 240B elemental analyzer. Molar conductivity measurements were carried out with a Crison Basic 30 conductometer. Room-temperature (RT) magnetic measurements were carried out by the Faraday method using mercury tetrathiocyanatocobaltate(II) as calibrant. Fluorescence spectra were recorded in solution on a Hitachi F-7000 fluorescence spectrophotometer. Viscosity experiments were carried out using an ALPHA L Fungilab rotational viscometer equipped with an 18 mL LCP spindle and the measurements were performed at 100 rpm.

Cyclic voltammetry studies were performed on an Eco chemie Autolab Electrochemical analyzer. Cyclic voltammetry experiments were carried out in a 30 mL three-electrode electrolytic cell. The working electrode was platinum disk, a separate Pt single-sheet electrode was used as the counter electrode and a Ag/AgCl electrode saturated with KCl was used as the reference electrode. The cyclic voltammograms of the complexes were recorded in 0.4 mM 1/2 DMSO/buffer solutions at $\nu = 100$ mV s^{-1} where buffer solution was the supporting electrolyte. Oxygen was removed by purging the solutions with pure nitrogen which had been previously saturated with solvent vapors. All electrochemical measurements were performed at 25.0 ± 0.2 °C.

2.2. Synthesis of the complexes

2.2.1. Synthesis of the complexes bearing N-donors, 1–6. Complexes **1–6** were prepared in a similar procedure. More specifically, a methanolic solution (5–10 mL) containing the potassium salt of the NSAID (generated *in situ* by the addition of KOH (0.4 mmol, 0.4 mL of 1 M solution) into a solution of the NSAID, *i.e.* Htolf, Hmef and Hnap) or the sodium salt of the NSAID (as it was commercially provided, *i.e.* Na meclf and Na dicl) (0.4 mmol) was added into a methanolic solution (~5 mL) of $CoCl_2 \cdot 6H_2O$ (0.2 mmol, 48 mg) followed by the addition of the corresponding N-donor co-ligand (Himi, py or 3-ampy). The solution was stirred vigorously for an hour and was left for slow evaporation at room temperature.

[Co(tolf)$_2$(Himi)$_2$], 1. Htolf (0.4 mmol, 104 mg) was used as the NSAID and Himi (0.4 mmol, 26 mg) was the N-donor used. Purple single-crystals of complex **1** suitable for X-ray crystallography were isolated after one week. Yield: 85 mg, 60%. Anal. calcd for $C_{34}H_{30}Cl_2CoN_6O_4$ (MW = 716.49): C 57.00, H 4.22, N 11.73; found: C 57.10, H 4.30, N 11.65%. IR (KBr disk), ν_{max}/cm^{-1}: $\nu_{asym}(COO)$: 1581 (vs); $\nu_{sym}(COO)$: 1385 (s); $\Delta\nu(COO) = 196$ cm^{-1}; $\rho(C–H)_{Himi} = 749$ (m). UV-vis: as nujol mull, λ/nm: 545; in DMSO solution, λ/nm (ε/M^{-1} cm^{-1}): 559 (150), 301 (15 000). $\mu_{eff} = 4.08$ BM at RT. The complex is soluble in DMSO and DMF and is non-electrolyte ($\Lambda_M = 12$ mho cm^2 mol^{-1} in 1 mM DMSO).

[Co(mef)$_2$(Himi)$_2$], 2. Hmef (0.4 mmol, 96 mg) was used as the NSAID and Himi (0.4 mmol, 26 mg) was the corresponding N-donor co-ligand. Purple-coloured single-crystals of complex **2** suitable for X-ray crystallography were isolated after ten days. Yield: 95 mg, 70%. Anal. calcd for $C_{36}H_{36}CoN_6O_4$ (MW = 675.65): C 64.00, H 5.37, N 12.44; found: C 64.10, H 5.45, N 12.30%. IR (KBr disk), ν_{max}/cm^{-1}: $\nu_{asym}(COO)$: 1577 (vs); $\nu_{sym}(COO)$: 1386 (s); $\Delta\nu(COO) = 191$ cm^{-1}; $\rho(C–H)_{Himi} = 747$ (m). UV-vis: as nujol mull, λ/nm: 540; in DMSO solution, λ/nm (ε/M^{-1} cm^{-1}): 557 (120), 334 (7000), 300 (13 000). $\mu_{eff} = 4.02$ BM at RT. The complex is soluble in DMSO and DMF and is non-electrolyte ($\Lambda_M = 11$ mho cm^2 mol^{-1} in 1 mM DMSO).

[Co(nap)$_2$(Himi)$_2$], 3. The synthesis of the complex was performed in acetonitrile. Hnap (0.4 mmol, 92 mg) was used as the NSAID and Himi (0.4 mmol, 26 mg) was the N-donor used as co-ligand. Purple-coloured microcrystalline product of complex **3** was collected after a few days. Yield: 80 mg, 60%. Anal. calcd for $C_{34}H_{34}CoN_4O_6$ (MW = 653.60): C 62.48, H 5.24, N 8.57; found: C 62.35, H 5.20, N 8.45%. IR (KBr disk), $\nu_{max}/$

cm^{-1}: $\nu_{asym}(COO)$: 1606 (vs); $\nu_{sym}(COO)$: 1390 (s); $\Delta\nu(COO) = 216\ cm^{-1}$; $\rho(C–H)_{Himi} = 755$ (m). UV-vis: as nujol mull, λ/nm: 572; in DMSO solution, $\lambda/nm\ (\varepsilon/M^{-1}\ cm^{-1})$: 581 (250), 332 (6100), 320 (12 200). $\mu_{eff} = 4.29$ BM at RT. The complex is soluble in DMSO and DMF and is non-electrolyte ($\Lambda_M = 15$ mho $cm^2\ mol^{-1}$ in 1 mM DMSO).

[Co(meclf)$_2$(Himi)$_2$], 4. Sodium meclofenamate (0.4 mmol, 126 mg) was used as the sodium salt of the NSAID and Himi (0.4 mmol, 26 mg) was the N-donor used as co-ligand. Purple-coloured microcrystalline product of complex **4** was collected after a few days. Yield: 95 mg, 60%. Anal. calcd for $C_{34}H_{28}Cl_4CoN_6O_4$ (MW = 785.38): C 52.00, H 3.59, N 10.70; found: C 51.85, H 3.45, N 10.60%. IR (KBr disk), ν_{max}/cm^{-1}: $\nu_{asym}(COO)$: 1583 (s); $\nu_{sym}(COO)$: 1393 (s); $\Delta\nu(COO) = 190\ cm^{-1}$; $\rho(C–H)_{Himi} = 749$ (m). UV-vis: as nujol mull, λ/nm: 559; in DMSO solution, $\lambda/nm\ (\varepsilon/M^{-1}\ cm^{-1})$: 555 (100), 317 (7500), 297 (13 900). $\mu_{eff} = 4.30$ BM at RT. The complex is soluble in DMSO and DMF and is non-electrolyte ($\Lambda_M = 11$ mho $cm^2\ mol^{-1}$ in 1 mM DMSO).

[Co(meclf)$_2$(py)$_2$(H$_2$O)$_2$]·2py, 5. Na meclf (0.4 mmol, 126 mg) was used as the sodium salt of the NSAID and pyridine (1.5 mL) was the N-donor used as co-ligand. Pink single-crystals of complex **5**, suitable for X-ray crystallography were isolated after three weeks. Yield: 110 mg, 55%. Anal. calcd for $C_{48}H_{44}Cl_4CoN_6O_6$ (MW = 1001.66): C 57.56, H 4.43, N 8.39; found: C 57.45, H 4.30, N 8.25%. IR (KBr disk), ν_{max}/cm^{-1}: $\nu_{asym}(COO)$: 1578 (vs); $\nu_{sym}(COO)$: 1387 (s); $\Delta\nu(COO) = 191\ cm^{-1}$; $\rho(C–H)_{py} = 698$ (m). UV-vis: as nujol mull, λ/nm: 530, 470; in DMSO solution, $\lambda/nm\ (\varepsilon/M^{-1}\ cm^{-1})$: 548 (50), 461 (95), 317 (6500), 300 (15 500). $\mu_{eff} = 4.35$ BM at RT. The complex is soluble in DMSO and DMF and is non-electrolyte ($\Lambda_M = 12$ mho $cm^2\ mol^{-1}$ in 1 mM DMSO).

{[Co(dicl)$_2$(3-ampy)(H$_2$O)$_3$][Co(dicl)$_2$(H$_2$O)$_4$]}, 6 (6a 6b). Sodium diclofenac (0.4 mmol, 127 mg) was used as the sodium salt of the NSAID and 3-ampy (0.2 mmol, 19 mg) was the corresponding N-donor co-ligand. Pink single-crystals of complex **6**, suitable for X-ray crystallography, were isolated after two weeks. Yield: 95 mg, 60%. Anal. calcd for $C_{30.5}H_{30}Cl_4CoN_3O_{7.5}$ (MW = 759.33): C 48.24, H 3.98, N 5.53; found: C 48.50, H 3.95, N 5.69%. IR (KBr disk), ν_{max}/cm^{-1}: $\nu_{asym}(COO)$: 1578 (vs); $\nu_{sym}(COO)$: 1381 (s); $\Delta\nu(COO) = 197\ cm^{-1}$; $\rho(C–H)_{3-ampy} = 809$ (m). UV-vis: as nujol mull, λ/nm: 545, 475; in DMSO solution, $\lambda/nm\ (\varepsilon/M^{-1}\ cm^{-1})$: 525 (40), 485 (35), 291 (8100). $\mu_{eff} = 3.93$ BM at RT. The complex is soluble in DMSO and DMF and is non-electrolyte ($\Lambda_M = 12$ mho $cm^2\ mol^{-1}$ in 1 mM DMSO).

2.2.2. Synthesis of complex [Co(meclf)$_2$(MeOH)$_4$], 7.

A methanolic solution (5 mL) containing Na meclf (0.4 mmol, 126 mg) was added into a methanolic solution (~5 mL) of CoCl$_2$·6H$_2$O (0.2 mmol, 48 mg). The reaction solution was stirred for two hours. Afterwards, it was left to evaporate slow at room temperature. Pink-coloured microcrystalline product of complex 7 was collected after a few days. Yield: 85 mg, 55%. Anal. calcd for $C_{32}H_{36}Cl_4CoN_2O_8$ (MW = 777.39): C 49.44, H 4.67, N 3.60; found: C 49.30, H 4.55, N 3.45%. IR (KBr disk), ν_{max}/cm^{-1}: $\nu_{asym}(COO)$: 1580 (vs); $\nu_{sym}(COO)$: 1389 (s); $\Delta\nu(COO)$

$= 191\ cm^{-1}$. UV-vis: as nujol mull, λ/nm: 540, 476; in DMSO solution, $\lambda/nm\ (\varepsilon/M^{-1}\ cm^{-1})$: 556 (10), 490 (35), 321 (8700), 299 (14 500). $\mu_{eff} = 3.97$ BM at RT. The complex is soluble in DMSO and DMF and is non-electrolyte ($\Lambda_M = 15$ mho $cm^2\ mol^{-1}$ in 1 mM DMSO).

2.2.3. Synthesis of the complexes bearing N,N′-donors, 8–14.

Complexes **8–13** were prepared following a similar procedure. More specifically, a methanolic solution (5–10 mL) containing the potassium salt of the NSAID (generated *in situ* by the addition of KOH (0.4 mmol, 0.4 mL of 1 M solution) into a solution of the NSAID, *i.e.* Htolf, Hmef and Hnap or the sodium salt of the NSAID (as it was commercially provided, *i.e.* Na meclf) (0.4 mmol) was added into a methanolic solution (~5 mL) of CoCl$_2$·6H$_2$O (0.2 mmol, 48 mg) followed by the addition of the corresponding N,N′-donor co-ligand (*i.e.* neoc, phen, bipy or bipyam). After 1 hour stirring, the reaction solution was left to evaporate slow at room temperature.

[Co(tolf)$_2$(neoc)], 8. Htolf (0.4 mmol, 104 mg) was used as the NSAID and neoc (0.2 mmol, 40 mg) was the N,N′-donor co-ligand used. In order to isolate single-crystals of the complex, the reaction solution was subjected to vapor diffusion with diethylether. Red-coloured single-crystals of complex **8**, suitable for X-ray crystallography, were isolated after one week. Yield: 100 mg, 65%. Anal. calcd for $C_{42}H_{34}Cl_2CoN_4O_4$ (MW = 788.59): C 63.97, H 4.35, N 7.10; found: C 63.80, H 4.25, N 7.00%. IR (KBr disk), ν_{max}/cm^{-1}: $\nu_{asym}(COO)$: 1580 (vs); $\nu_{sym}(COO)$: 1406 (s); $\Delta\nu(COO) = 174\ cm^{-1}$; $\rho(C–H)_{neoc} = 729$ (m). UV-vis: as nujol mull, λ/nm: 537, 475; in DMSO solution, $\lambda/nm\ (\varepsilon/M^{-1}\ cm^{-1})$: 550 (80), 490 (65), 296 (17 000). $\mu_{eff} = 4.27$ BM at RT. The complex is soluble in DMSO and DMF and is non-electrolyte ($\Lambda_M = 16$ mho $cm^2\ mol^{-1}$ in 1 mM DMSO).

[Co(mef)$_2$(neoc)], 9. Hmef (0.4 mmol, 96 mg) was used as the NSAID and neoc (0.2 mmol, 40 mg) was the N,N′-donor co-ligand used. Vapor diffusion with diethylether of the reaction solution resulted in the formation of brownish single-crystals of complex **9**, suitable for X-ray crystallography after ten days. Yield: 90 mg, 60%. Anal. calcd for $C_{44}H_{40}CoN_4O_4$ (MW = 747.76): C 70.68, H 5.39, N 7.49; found: C 70.55, H 5.28, N 7.35%. IR (KBr disk), ν_{max}/cm^{-1}: $\nu_{asym}(COO)$: 1581 (vs); $\nu_{sym}(COO)$: 1401 (s); $\Delta\nu(COO) = 180\ cm^{-1}$; $\rho(C–H)_{neoc} = 732$ (m). UV-vis: as nujol mull, λ/nm: 555, 480; in DMSO solution, $\lambda/nm\ (\varepsilon/M^{-1}\ cm^{-1})$: 560 (55), 485 (35), 348 (6400), 311 (14 200). $\mu_{eff} = 4.31$ BM at RT. The complex is soluble in DMSO and DMF and is non-electrolyte ($\Lambda_M = 16$ mho $cm^2\ mol^{-1}$ in 1 mM DMSO).

[Co(nap)$_2$(neoc)], 10. The synthesis of the complex was performed in acetonitrile. Hnap (0.4 mmol, 92 mg) was used as the NSAID and neoc (0.2 mmol, 40 mg) was the N,N′-donor co-ligand used. Purple single-crystals of complex **10**, suitable for X-ray crystallography, were isolated after one week. Yield: 95 mg, 65%. Anal. calcd for $C_{42}H_{38}CoN_2O_6$ (MW = 725.71): C 69.51, H 5.28, N 3.86; found: C 69.40, H 5.20, N 3.70%. IR (KBr disk), ν_{max}/cm^{-1}: $\nu_{asym}(COO)$: 1575 (vs); $\nu_{sym}(COO)$: 1393 (s); $\Delta\nu(COO) = 182\ cm^{-1}$; $\rho(C–H)_{neoc} = 731$ (m). UV-vis: as nujol mull, λ/nm: 582, 480; in DMSO solution, $\lambda/nm\ (\varepsilon/M^{-1}\ cm^{-1})$: 590 (75), 475 (50), 333 (5900), 318 (13 500). $\mu_{eff} = 4.24$ BM at

RT. The complex is soluble in DMSO and DMF and is non-electrolyte (Λ_M = 15 mho cm^2 mol^{-1} in 1 mM DMSO).

[Co(meclf)$_2$(phen)], 11. Na meclf (0.4 mmol, 126 mg) was used as the sodium salt of the NSAID and phen (0.2 mmol, 36 mg) was the corresponding N,N′-donor co-ligand. Pink microcrystalline product of complex **11** was collected after a few days. Yield: 100 mg, 60%. Anal. calcd for C$_{40}$H$_{28}$Cl$_4$CoN$_4$O$_4$ (MW = 829.43): C 57.92, H 3.40, N 6.75; found: C 57.80, H 3.25, N 6.65%. IR (KBr disk), ν_{max}/cm^{-1}: ν_{asym}(COO): 1580 (vs); ν_{sym}(COO): 1416 (s); $\Delta\nu$(COO) = 164 cm^{-1}; ρ(C–H)$_{phen}$ = 728 (m). UV-vis: as nujol mull, λ/nm: 562, 485; in DMSO solution, λ/nm (ε/M^{-1} cm^{-1}): 550 (40), 476 (55), 316 (6900), 292 (16 700). μ_{eff} = 4.30 BM at RT. The complex is soluble in DMSO and DMF and is non-electrolyte (Λ_M = 12 mho cm^2 mol^{-1} in 1 mM DMSO).

[Co(meclf)$_2$(bipy)], 12. Na meclf (0.4 mmol, 126 mg) was used as the sodium salt of the NSAID and bipy (0.2 mmol, 31 mg) was the corresponding N,N′-donor co-ligand. Brownish microcrystalline product of complex **12** was collected after a few days. Yield: 95 mg, 60%. Anal. calcd for C$_{38}$H$_{28}$Cl$_4$CoN$_4$O$_4$ (MW = 805.41): C 56.67, H 3.50, N 6.96; found: C 56.55, H 3.40, N 6.85%. IR (KBr disk), ν_{max}/cm^{-1}: ν_{asym}(COO): 1579 (vs); ν_{sym}(COO): 1415 (s); $\Delta\nu$(COO) = 164 cm^{-1}; ρ(C–H)$_{bipy}$ = 763 (m). UV-vis: as nujol mull, λ/nm: 565, 475; in DMSO solution, λ/nm (ε/M^{-1} cm^{-1}): 560 (20), 485 (50), 328 (7100), 289 (17 500). μ_{eff} = 4.19 BM at RT. The complex is soluble in DMSO and DMF and is non-electrolyte (Λ_M = 5 mho cm^2 mol^{-1} in 1 mM DMSO).

[Cao(meclf)$_2$(bipyam)], 13. Na meclf (0.4 mmol, 126 mg) was used as the sodium salt of the NSAID and bipyam (0.2 mmol, 34 mg) was the corresponding N,N′-donor co-ligand. Orange microcrystalline product of complex **13** was collected after two weeks. Yield: 105 mg, 65%. Anal. calcd for C$_{38}$H$_{29}$Cl$_4$CoN$_5$O$_4$ (MW = 820.43): C 55.63, H 3.56, N 8.54; found: C 55.50, H 3.45, N 8.40%. IR (KBr disk), ν_{max}/cm^{-1}: ν_{asym}(COO): 1586 (vs); ν_{sym}(COO): 1420(s); $\Delta\nu$(COO) = 166 cm^{-1}; ρ(C–H)$_{bipyam}$ = 770 (m). UV-vis: as nujol mull, λ/nm: 543, 469; in DMSO solution, λ/nm (ε/M^{-1} cm^{-1}): 548 (15), 480 (65), 318 (7800), 296 (13 700). μ_{eff} = 4.25 BM at RT. The complex is soluble in DMSO and DMF and is non-electrolyte (Λ_M = 11 mho cm^2 mol^{-1} in 1 mM DMSO).

[Co$_2$(difl)$_2$(neoc)$_2$]·MeOH, 14. For the synthesis of complex **14**, a methanolic solution of H$_2$difl (0.2 mmol, 50 mg) containing KOH (0.4 mmol, 0.4 mL of 1 M) was stirred for 1 h at RT. The reaction solution was added into the methanolic solution of solution (~5 mL) of CoCl$_2$·6H$_2$O (0.2 mmol, 48 mg) simultaneously with neoc (0.2 mmol, 40 mg). Brown well-shaped single-crystals of complex **14**, suitable for X-ray crystallography, were isolated after three days. Yield: 60 mg, 55%. Anal. calcd for C$_{55}$H$_{40}$Co$_2$F$_4$N$_4$O$_7$ (MW = 1062.80): C 62.16, H 3.79, N 5.27; found: C 62.00, H 3.65, N 5.15%. IR (KBr disk), ν_{max}/cm^{-1}: ν_{asym}(COO): 1588 (vs); ν_{sym}(COO): 1398 (s); $\Delta\nu$(COO) = 190 cm^{-1}; ρ(C–H)$_{neoc}$ = 730 (m). UV-vis: as nujol mull, λ/nm: 548, 467; in DMSO solution, λ/nm (ε/M^{-1} cm^{-1}): 555 (35), 475 (75), 319 (6500), 296 (11 000). The complex is soluble in DMSO and DMF and is non-electrolyte (Λ_M = 13 mho cm^2 mol^{-1} in 1 mM DMSO).

2.3. X-ray structural determination

Single-crystals of the complexes suitable for crystal structure analysis were mounted at room temperature on a Bruker Kappa APEX2 diffractometer equipped with a Triumph monochromator using Mo Kα (λ = 0.71073 Å, source operating at 50 kV and 30 mA) radiation. Unit cell dimensions were determined and refined by using the angular settings of at least 188 high intensity reflections (>10σ(I)) in the range 10° < 2θ < 20°. Intensity data were recorded using φ and ω-scans. All crystals presented no decay during the data collection. The frames collected were integrated with the Bruker SAINT Software package[66] using a narrow-frame algorithm. Data were corrected for absorption using the numerical method (SADABS) based on crystal dimensions.[67] The structures were solved using SUPERFLIP[68] incorporated in Crystals. Data refinement (full-matrix least-squares methods on F^2) and all subsequent calculations were carried out using the Crystals version 14.61 build 6236 program package.[69] All non-hydrogen non-disordered atoms were refined anisotropically. For the disordered atoms, their occupation factors were first refined under fixed isotropic parameters. Their isotropic displacement factors were finally refined under the fixed occupation factors previously observed. Hydrogen atoms bonded to non-disordered atoms were located from difference Fourier maps and refined using soft constraints at idealised positions riding on the parent atoms with isotropic displacement parameters U_{iso}(H) = 1.2U_{eq}(C) and 1.5U_{eq} (–NH and –OH hydrogens) at distances C–H 0.95 Å, N–H 0.84 Å and O–H 0.82 Å. Both NH and OH hydrogen atoms were allowed to rotate. For the disordered hydrogen atoms with disordered parent atoms, their positions were selected to fulfil the previous demands as well as the hydrogen bonding demands when necessary.

Crystallographic data for the complexes are presented in Tables S1–S4.† Further details on the crystallographic studies as well as atomic displacement parameters are given as ESI† in the form of cif files.

2.4. *In vitro* biological activity studies

In order to study *in vitro* the biological activity (*i.e.*, antioxidant activity and interaction with DNA or albumins) of complexes **1–14**, the complexes were initially dissolved in DMSO (1 mM). Mixing of such solutions with the aqueous buffer solutions of the biomacromolecules (DNA or albumins) never exceeded 5% DMSO (v/v) in the final solution, which was needed due to low aqueous solubility of most compounds. Control experiments with DMSO were performed and no significant effect on the measurements was observed.

The antioxidant activity of the complexes was evaluated by determining their ability to scavenge DPPH and ABTS free radicals (expressed as percentage of radical scavenging, DPPH% and ABTS%, respectively) and to reduce H$_2$O$_2$. The interaction of the complexes with CT DNA was investigated by UV-vis spectroscopy, viscosity measurements, and cyclic voltammetry and *via* the evaluation of their EB-displacing ability which was monitored by fluorescence emission spectroscopy. The serum

albumin (BSA or HSA) binding studies were performed by tryptophan fluorescence quenching experiments in the absence or presence of the albumin site-markers warfarin and ibuprofen. Detailed procedures regarding the *in vitro* study of the biological activity of the complexes are given in the ESI (sections S1–S4†).

3. Results and discussion

3.1. Synthesis and characterisation

The complexes were synthesised in high yield *via* the aerobic reaction of a methanolic solution of the corresponding deprotonated NSAID with $CoCl_2 \cdot 6H_2O$ and the corresponding N-donor co-ligand (Himi, py or 3-ampy) in a $1:2:2$ $Co^{2+} : NSAID^{-1} : (N$-donor) ratio for complexes **1–6**. In a similar manner, the use of corresponding N,N′-donor co-ligand (neoc, bipy, phen or bipyam) in a $1:2:1$ $Co^{2+} : NSAID^{-1} : (N,N'$-donor) ratio afforded complexes **8–13**. For complex **14**, a $1:1:1$ $Co^{2+} : difl^{-2} : neoc$ ratio was used, while a $1:2$ $Co^{2+} : meclf^{-1}$ ratio yielded complex **7**.

The complexes were characterised by IR and UV-vis spectroscopy, RT-magnetic measurements and X-ray crystallography (for eight of the fourteen complexes X-ray crystal structures were determined). The proposed formulas of the complexes were based on the results of elemental analysis. The complexes are stable in the air, soluble in DMSO and DMF and insoluble in most organic solvents and H_2O.

According to the molar conductivity values (Λ_M = 5–16 mho cm^2 mol^{-1} for 1 mM DMSO solution), the complexes are non-electrolytes in DMSO solution (in the case of a $1:1$ electrolyte, the Λ_M value of a 1 mM DMSO solution should be higher than 70 mho cm^2 mol^{-1})[70] and do not dissociate in solution keeping their integrity. From the magnetic measurements of the mononuclear complexes **1–13** at RT, the obtained μ_{eff} values were in the range 3.93–4.35 BM and are higher than the expected spin-only value (μ_{eff} = 3.87 BM) as expected for mononuclear high-spin Co(II) complexes.[71]

IR spectroscopy was used to confirm the existence of the NSAID ligands and nitrogen-donor co-ligands in the complexes. In the IR spectra of the complexes, two intense bands attributable to the characteristic stretching vibrations of their carboxylate group, *i.e.* the antisymmetric ($\nu_{asym}(COO)$) and the symmetric ($\nu_{sym}(COO)$) were observed in the regions 1578–1606 cm^{-1} and 1381–1420 cm^{-1}, respectively. The parameter $\Delta\nu(COO)$ is usually used to suggest the coordination mode of the carboxylato group of a ligand when compared to its salt. For complexes **1–7**, and **14**, the values of $\Delta\nu(COO)$ were in the range 190–216 cm^{-1} and are higher than that of the corresponding NSAID salt revealing a monodentate coordination mode.[72] For complexes **8–13**, bidentate chelating mode was concluded since the $\Delta\nu(COO)$ values were found in the range 164–182 cm^{-1} and were lower were than $\Delta\nu(COO)$ of the corresponding NSAID salt.[72] Furthermore, the co-existence of the corresponding nitrogen-donor co-ligands in the complexes was verified by the presence of the characteristic bands attribu-

ted to the out-of-plane $\rho(C–H)$ vibrations found at 747–755 cm^{-1} for $\rho(C–H)_{Himi}$ in **1–4**, 698 cm^{-1} for $\rho(C–H)_{py}$ in **5**, 809 cm^{-1} for $\rho(C–H)_{3-ampy}$ in **6**, 729–732 cm^{-1} for $\rho(C–H)_{neoc}$ in **8–10** and **14**, 728 cm^{-1} for $\rho(C–H)_{phen}$ in **11**, 763 cm^{-1} for $\rho(C–H)_{bipy}$ in **12**, and 770 cm^{-1} for $\rho(C–H)_{bipyam}$ in **13**.[72] Such features regarding the coordination of the carboxylato group of the NSAID ligands and the presence of the nitrogen-donor co-ligands are in good agreement with the crystal structures of the complexes determined and discussed in section 3.2.

The electronic (UV-vis) spectra of the complexes were recorded as nujol mull and in DMSO solution and were found similar suggesting that the complexes retain their structure in solution. In the visible region of the spectrum: for complexes **1–4**, one band assigned to d–d transition ($^4A_2 \rightarrow {}^4T_1(P)$) was observed in the range 555–581 nm (ε = 100–250 M^{-1} cm^{-1}) which is typical for tetrahedral Co(II) complexes,[71] and for complexes **5–14**, two low-intensity d–d bands were observed in region 525–590 nm (ε = 10–80 M^{-1} cm^{-1}) and 461–490 nm (ε = 35–95 M^{-1} cm^{-1}) attributable to $^4T_{1g}(F) \rightarrow {}^4A_{2g}$ and $^4T_{1g}(F) \rightarrow {}^4T_{1g}(P)$ transitions,[71] respectively. It may be noted that the ε values of the d–d transition bands for the four-coordinate Co(II) complexes **1–4** are higher than those of the six-coordinate Co(II) complexes **5–14**, as expected.[71] In addition, one or two bands in the range 289–334 nm assigned to intra-ligand transitions were observed in the UV region of the spectra.

### 3.2. Structural characterisation of the complexes

Continuous attempts in order to obtain single-crystals of the complexes suitable for X-ray crystallography were successful for eight of the complexes, namely complexes **1, 2, 5–9** and **13**. For the rest six complexes, their structural characterisation was based on the other techniques used.

3.2.1. Structure of the complexes bearing N-donors, complexes 1–6. Complexes **1** (CCDC 2336775) and **2** (CCDC 2336776)† bear the same general formula $[Co(NSAID)_2(Himi)_2]$, however they have some differences arising from the coordination mode of the NSAID ligands. Both complexes crystallised in monoclinic crystal system and $P2_1/n$ space group (Table S1†). Their molecular structures are depicted in Fig. 3 and selected bond distances and angles are summarised in Table S5.†

In complex **1**, the tolfenamato ligands are coordinated to cobalt(II) ion in a monodentate manner through O1 and O3 atoms with Co–O distances 1.980(2) Å and 2.0078(18) Å, respectively. The distances of the non-coordinated carboxylato oxygen atoms O2 and O4 from Co1 are 2.985 Å and 2.559 Å, respectively. The two imidazole ligands are neutral and coordinated to Co1 through N1 and N3 atoms (Co–N = 2.048(2) Å and 2.025(2) Å, respectively). Quite similar is the arrangement of the NSAID and imidazole ligands around Co(II) ion in complexes $[Co(dicl)_2(Himi)_2]$[42] and $[Co(indo)_2(Himi)_2]$[73] where Hindo is the NSAID indomethacin.

In order to check the geometry around four-coordinated Co1, the following structural parameters were calculated: (a) the tetrahedrality (it can be determined from the angle formed by the two planes enclosing the cobalt ion and two adjacent
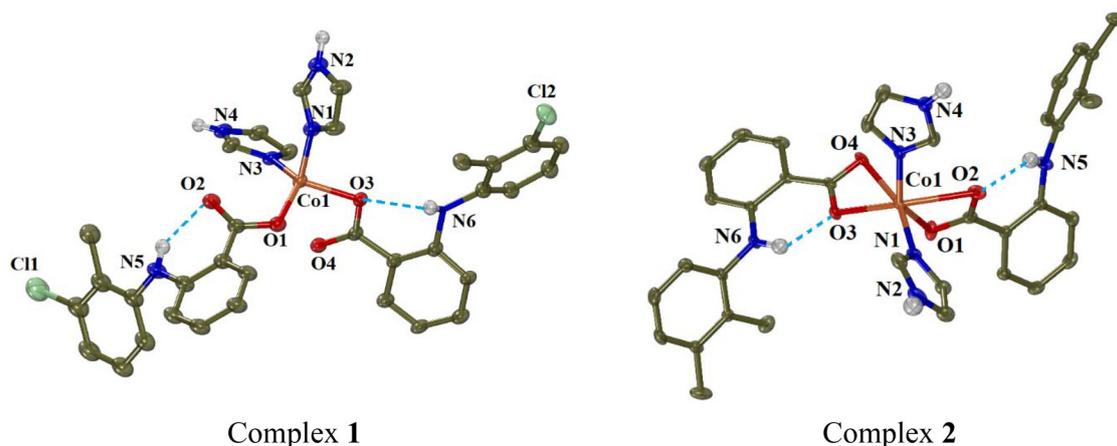
Complex **1**   Complex **2**

Fig. 3 Molecular structures of complexes **1** and **2**. Methyl and aromatic hydrogen atoms are omitted for clarity. The intra-ligand H-bonds are shown in light-blue dot lines.

coordinated atoms; in case of strictly square planar complexes (D_{4h} symmetry), the tetrahedrality equals 0°; for tetrahedral complexes (D_{2d} symmetry), the tetrahedrality is 90°),[74] and (b) the tetrahedral index as introduced by Yang ($\tau_4 = (360° - (\alpha + \beta))/(360° - 2 \times 109.5°)$, where α and β are the largest angles around the metal)[75] or as introduced by Okuniewski ($\tau'_4 = ((\beta - \alpha)/(360° - 109.5°)) + ((180° - \beta)/(180° - 109.5°))$ where $\beta > \alpha$ are the largest angles of the coordination sphere).[76] For complex **1**, the tetrahedrality (as determined by the dihedral angle of planes formed by atoms O1, Co1, N1 and O3, Co1, N3) has a value of 87.80° (which is close to 90°) and the tetrahedral indexes are close to 1 ($\tau_4 = 0.85$ and $\tau'_4 = 0.81$); all these values support tetrahedral geometry for the chromophore CoO$_2$N$_2$.

In complex **2**, the mefenamato ligands are bound to Co1 ion in an asymmetric bidentate mode with two short Co–O bond distances (2.042(2) Å and 2.025(2) Å) and two much longer distances (2.420(3) Å and 2.435(3) Å). In such a case, Co1 could be considered six-coordinate, its coordination sphere (CoN$_2$O$_4$) is completed by N1 and N3 of the imidazole ligands (2.035(2)–2.051(3) Å) and its geometry would be described as a distorted octahedron (with the largest angles O4–Co1–N1 = 162.02(9)°, O2–Co1–O3 = 156.90(9)° and O1–Co1–N3 = 143.01(11)° revealing the distortion). However, the Co1–O2 and Co1–O4 distances can be considered too long for a bonding distance; subsequently, Co1 is four-coordinate, and the structural parameters tetrahedrality, τ_4 and τ'_4 have values 79.23, 0.80 and 0.68, respectively, suggesting a distorted tetrahedral geometry around Co1, which is in good agreement with electronic spectra discussed in section 3.1. It should be noted that a structure of complex [Co(mef)$_2$(Himi)$_2$] has been recently reported.[46] That structure is similar to that of complex **2**, with the difference that the reported structure was centrosymmetric.[46]

The structures of both complexes are further stabilised by the formation of intraligand and intermolecular hydrogen-bonds between the amino hydrogen of the NSAID (tolfenamato or mefenamato) ligands and their carboxylato oxygens in the same ligand or in neighbouring complexes (Table S6†).

Complexes **3** and **4** are isostructural with complexes **1**, **2**, [Co(dicl)$_2$(Himi)$_2$][42] and [Co(indo)$_2$(Himi)$_2$],[73] and are expected to have similar structural features: they are mononuclear (μ_{eff} = 4.29–4.40 BM), with the naproxen and meclofenamato ligands, respectively, monodentately bound to Co(II) ion via a carboxylato oxygen atom ($\Delta\nu$(COO) = 190–216 cm^{-1}) and contain two co-ordinated imidazole co-ligands (ρ(C–H)$_{Himi}$ = 749–755 cm^{-1}). The Co(II) ions are four-coordinate with a CoN$_2$O$_2$ chromophore and a distorted tetrahedral geometry (Fig. 4).

Complex **5** (CCDC 2336777†) crystallised in triclinic crystal system and $P\bar{1}$ space group (Table S2†). In complex **5**, the meclofenamato ligands are coordinated monodentately to Co(II) ion. Two pyridine solvate molecules were also found in the unit cell. The molecular structure of complex **5** is depicted in Fig. 5 and selected bond distances and angles are cited in Table S7.†

The structure of complex **5** is centrosymmetric, with the cobalt(II) ion (Co1) being on the centre of symmetry and bound to two meclofenamato, two pyridine and two aqua ligands having a distorted octahedral geometry. The basal plane of the octahedron consists of the carboxylate oxygen atoms O1 and O1^i and the aqua oxygen atoms O3 and O3^i while the pyridine nitrogen atoms N1 and N1^i are located at the axial positions at 2.201(3) Å. In the equatorial CoO$_4$ plane of the octahedron, the bond distances Co–O$_{carb}$ (Co1–O1 = 2.094(2) Å) and Co–O$_{aqua}$ (Co1–O3 = 2.097(2) Å) are similar. The uncoordinated carboxylate oxygen atoms O2 and O2^i are lying at Co1···O2 distance of 3.38 Å. Similar arrangement of the NSAID, pyridine and aqua ligands around the cobalt(II) ion was observed in the structures of complexes [Co(dicl)$_2$(py)$_2$(H$_2$O)$_2$][42] and [Co(nap)$_2$(py)$_2$(H$_2$O)$_2$],[16] although the latter is not centrosymmetric.

A series of hydrogen bonds contribute to further stabilisation of the structure of complex **5**; intra-ligand H-bonds are
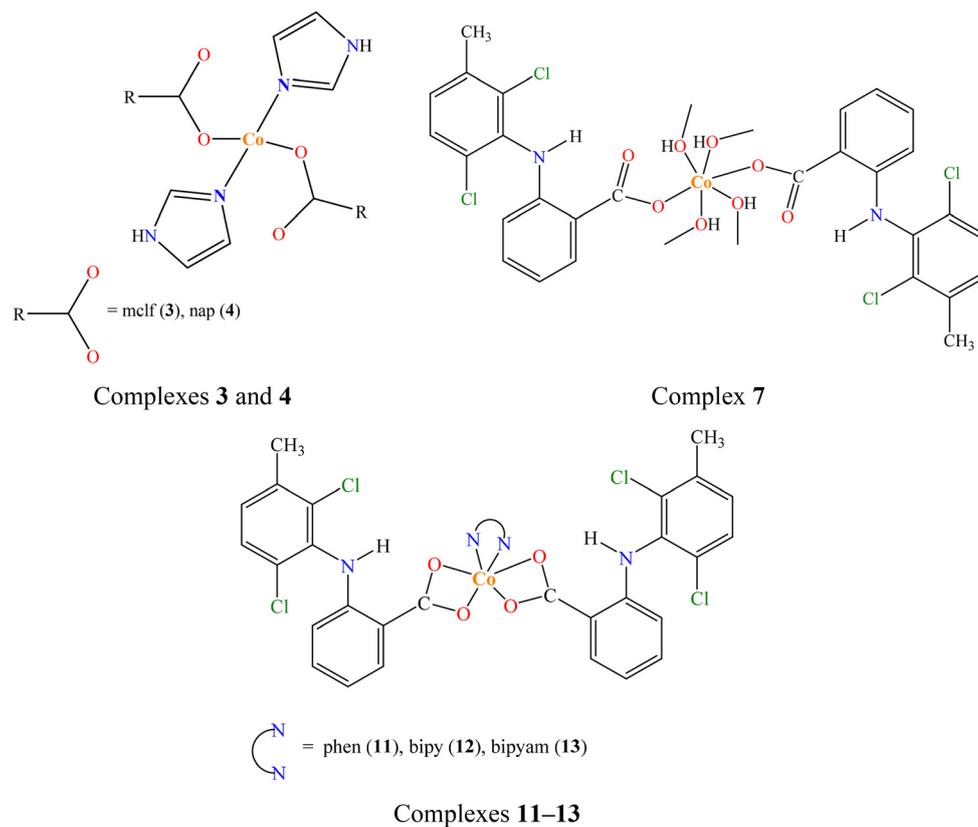
Complexes **3** and **4**

Complex **7**

= phen (**11**), bipy (**12**), bipyam (**13**)

Complexes **11–13**

Fig. 4 Proposed structures for complexes **3**, **4**, **7** and **11–13**.
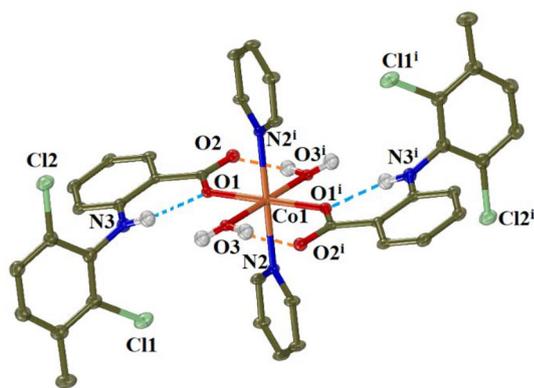

Fig. 5 Molecular structure of complex **5** (symmetry code: (i) $-x + 1$, $-y + 1$, $-z + 1$). Aromatic hydrogen atoms, and solvate molecules are omitted for clarity. The intra-ligand and intramolecular H-bonds are shown in light-blue and orange dot lines, respectively.

developed between the amino H atoms and the coordinated carboxylato oxygens O1, intramolecular H-bonds are formed between aqua H atoms and the non-coordinated carboxylato oxygen atoms O2, and intermolecular H-bonds between aqua H atoms and the nitrogen atoms of solvate pyridines (Table S6†).

Complex **6** (CCDC 2336778†) crystallised in monoclinic crystal system and $C2/c$ space group (Table S2†). The asymmetric unit comprises the half of a cobalt(II) complex with the metal atom on a special position, one fully occupied diclofenac ligand, three aqua ligands with occupation factors of $\frac{1}{2}$ and finally one more aqua ligand as well as an aminopyridine ligand with occupations of $\frac{1}{4}$. From the four complexes present in the unit cell, two of them were found to have the general formula $[Co(dicl)_2(3\text{-ampy})(H_2O)_3]$ (namely **6a**) and the rest two were found formulated as $[Co(dicl)_2(H_2O)_4]$ (namely **6b**). The molecular structures of the mononuclear complexes **6a** and **6b** are given in Fig. 6 and selected bond distances and angles are summarised in Table S8.†

In both complexes **6a** and **6b**, the cobalt(II) ions are six-coordinated and the diclofenac ligands are coordinated in a monodentate fashion. In the case of **6a**, the Co(II) ion is bound to two carboxylato oxygen atoms O1 and O1^i, three aqua oxygen atoms O5, O5^i and O6 and the aromatic nitrogen atom N2 (aqua O6 and the 3-aminopyridine ligand being disordered over two positions with equal occupation factors). In the case of **6b**, the coordination sphere comprises the oxygen atoms of the diclofenac ligands O1 and O1^i and four aqua oxygen atoms O3, O3^i, O4 and O4^i. So the chromophores are CoNO$_5$ in **6a** and CoO$_6$ in **6b**, resulting in a distorted octahedral geometry around Co1 in both cases. The bonding distances around Co1 ion in both cases are in the range 2.065(12)–2.170(14) Å, while the non-coordinated diclofenac O2 atoms are lying at 3.280 Å away from Co1.
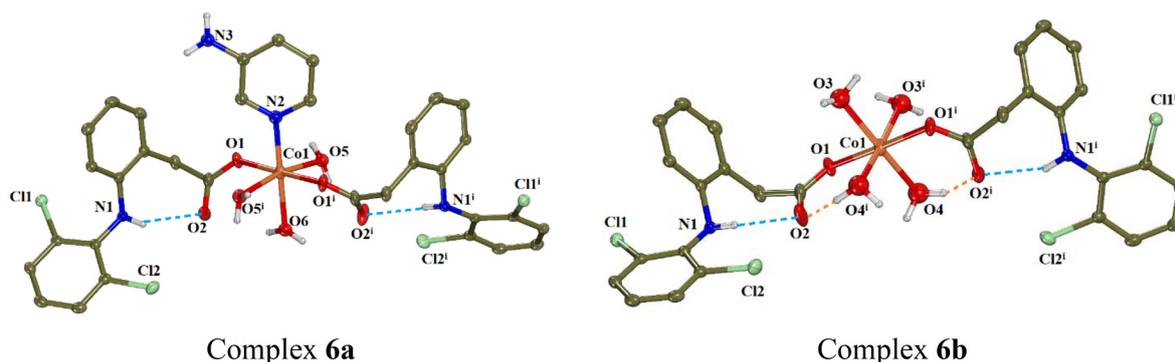
Complex 6a

Complex 6b

Fig. 6 Molecular structures of complexes **6a** and **6b** (symmetry code: (i) −x + 1, y, −z + 1/2). Methyl and aromatic hydrogen atoms are omitted for clarity. The intra-ligand and intramolecular H-bonds are shown in light-blue and orange dot lines, respectively.

The non-coordinated carboxylato oxygen O2 of diclofenac ligand participates in the formation of intraligand H-bonds with the diclofenac amino H atoms and intramolecular H-bonds with the aqua H atoms contributing to further stabilisation of the structure. Further intermolecular H-bonds are developed between aqua H atoms and the coordinated carboxylato oxygens O1 from adjacent molecules (Table S6†).

3.2.2. Structure of the complexes bearing N,N′-donors, complexes 8–14. Complexes **8–13** bear the same general formula [Co(NSAID)$_2$(N,N′-donor)], but only the structures of complexes **8–10** with the formula [Co(NSAID)$_2$(neoc)] were characterised by X-ray crystallography. Complexes **8** (CCDC 2336779) and **10** (CCDC 2336781)† crystallised in monoclinic crystal system and $P2_1/c$ space group, while complex **9** (CCDC 2336780†) crystallised in triclinic crystal system and $P\bar{1}$ space group (Tables S3 and S4†). The molecular structures of complexes **8–10** are depicted in Fig. 7 and selected bond distances and angles are summarised in Table S9.†

These three structures bear similarities and are discussed together. In the mononuclear complexes, the NSAID ligands (tolfenamato in **8**, mefenamato in **9**, and naproxen in **10**) are coordinated to cobalt(II) ion in an asymmetric bidentate chelating mode through their two carboxylato oxygen atoms. The six-coordinate Co(II) is surrounded by two NSAID ligands and one bidentate neoc ligand completing a CoN$_2$O$_4$ chromophore and shows a distorted octahedral geometry (largest angle 166.11(8)° in **8**, 164.11(6)° in **9**, and 160.99(9)° in **10**) where two N and four O atoms lying at the vertices of the octahedron. In complexes **8** and **9**, the asymmetric bidentate mode is obvious from the differences in the Co1–O bond distances; for each NSAID ligand, there is a short Co1–O distance (2.0630 (15)–2.1105(19) Å) and a longer one (2.1869(17)–2.2472(15) Å). In complex **10**, the case is similar for one naproxen ligand (Co1–O1 = 2.031(2) Å and Co1–O2 = 2.260(2) Å), while for the second naproxen ligand the Co1–O bond distances are much closer (2.151(2) Å and 2.172(2) Å). In all three complexes, the Co1–N bond distances are in the range 2.0966(18)–2.126(2) Å. The structures of complexes **8** and **9** are further stabilised by the development of intraligand hydrogen-bonds between the amino group of tolfenamato and mefenamato ligands, respectively, and their coordinated carboxylato group (Table S6†).

The structures of complexes **8** and **9** are similar but not identical with those previously reported by Smolkova *et al.*[44,45] However, there are some crystallographic differences. Complex **8** crystallised in different crystal system and space group from the reported complex [Co(tolf)$_2$(neoc)] (orthorhombic crystal system and $Pna2_1$ space group) which contained three crystallographically independent units.[45] For the reported complex [Co(mef)$_2$(neoc)], three differently coloured and shaped crystal polymorphs were isolated and characterised,[44] which was not observed for complex **9**. In addition, the structures were resolved in slightly different temperatures. The arrangement of the ligand atoms around cobalt(II) ion observed in complexes **8–10** is similar with that reported for isostructural complexes of the formula [Co(NSAID)$_2$(N,N′-donor)], such as [Co(dicl)$_2$(-bipy)], [Co(dicl)$_2$(bipyam)] and [Co(dicl)$_2$(phen)],[42] [Co(flufenamato)$_2$(bipyam)] and [Co(mef)$_2$(bipyam)],[43] [Co(tolf)$_2$(bipyam)],[41] and [Co(fenamato)$_2$(neoc)].[45]

Complexes **11–13** are expected to have similar structural features with complexes **8–10** and those reported in the literature.[41–45] They are mononuclear complexes (μ_{eff} = 4.19–4.30 BM) with the meclofenamato ligands bound to Co(II) ions in an asymmetrical bidentate chelating mode ($\Delta\nu$(COO) = 164–166 cm^{-1}) and contain a N,N′-donor (phen in **11** (ρ(C–H)$_{phen}$ = 728 cm^{-1}), bipy in **12** (ρ(C–H)$_{bipy}$ = 763 cm^{-1}), and bipyam in **13** (ρ(C–H)$_{bipyam}$ = 770 cm^{-1})) as co-ligand. The Co(II) ions are six-coordinate with CoN$_2$O$_4$ chromophore and distorted octahedral geometry (Fig. 4).

Complex **14** (CCDC 2336782†) crystallised in monoclinic crystal system and $C2/c$ space group (Table S4†). The molecular structure of complex **14** is shown in Fig. 8 and selected bond distances and angles are summarised in Table S10.† A methanol solvate molecule was found in the unit cell.

In this centrosymmetric dinuclear Co(II) complex, the centre of symmetry is lying on the middle of the interatomic distance between the two cobalt(II) ions. The diflunisal ligands are doubly deprotonated and are coordinated to the cobalt ions in a tridentate bridging mode, *i.e. via* the phenolato
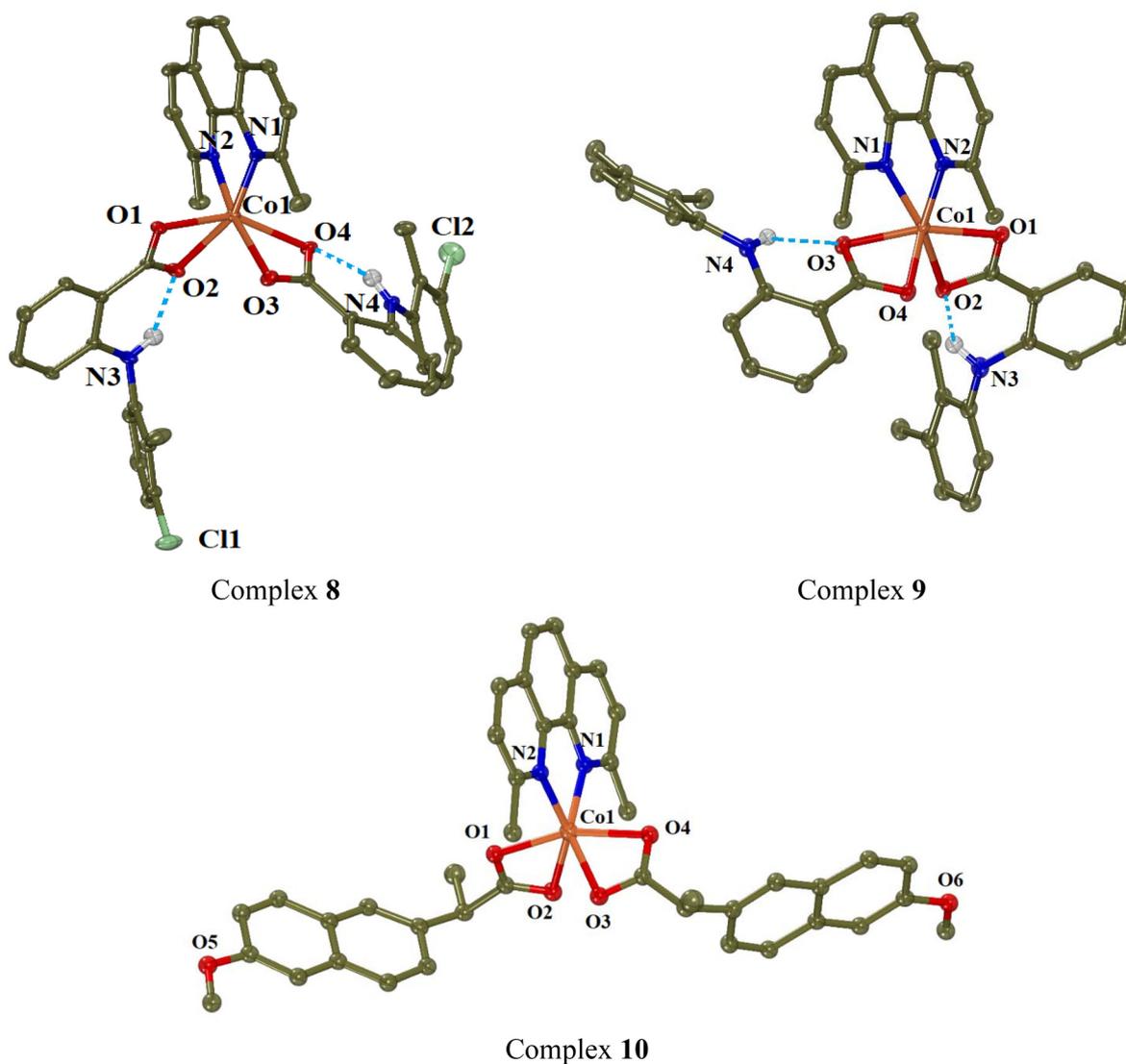
Fig. 7 Molecular structures of complexes 8–10. Methyl and aromatic hydrogen atoms are omitted for clarity. The intra-ligand H-bonds are shown in light-blue dot lines.
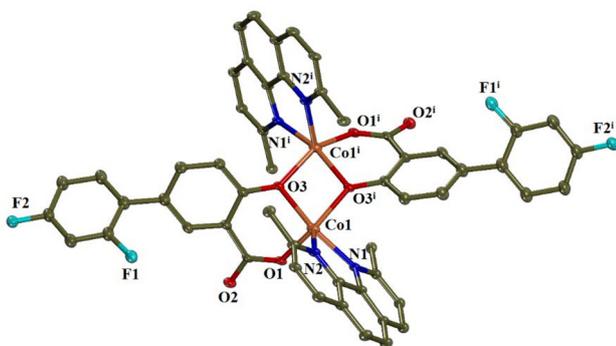
Fig. 8 Molecular structure of complex 14. Methyl and aromatic hydrogen atoms, as well as solvate methanol molecules are omitted for clarity.

oxygen atom O3 which bridges the two cobalt ions Co1 and Co1^i and a carboxylato oxygen atom O1 which participate in the formation of a six-membered chelate ring. Although such coordination mode is rather usual for salicylato ligands,[77–83] this is the first case reported for diflunisal ligands being in a tridentate bridging mode. There are also two complexes bearing doubly deprotonated diflunisal ligands which are co-ordinated in a bidentate chelating mode; an iron(III) dinuclear complex where the diflunisal ligands are terminal[40] and a gallium(III) mononuclear compound.[84] It should be also noted that a series of dinuclear copper(II) complexes with the general formula [Cu$_2$(salicylato)$_2$(N,N′-donor)$_2$] have similar structural features with complex 14.[81,85,86]

Each Co(II) is five-coordinate with a CoN$_2$O$_3$ chromophore formed by two bridging phenolato oxygen atoms, one carboxy-lato oxygen atom and two nitrogen atoms from the neoc

ligands. The geometry around cobalt(II) ions can be described as distorted square pyramid, according to the value of the trigonality index $\tau_5 = (159.05(9)° − 144.43(10)°)/60° = 0.244$ ($\tau_5 = (\varphi_1 − \varphi_2)/60°$, with φ_1 and φ_2 being the largest angles in the coordination sphere; $\tau_5 = 0$ is found for a perfect square pyramid and $\tau_5 = 1$ is calculated for a perfect trigonal bipyramid[87]). Based on the largest angles around Co1, atoms O1, O3, O3^i, and N1 form the basal plane of the square pyramid, and N2 lies on the apical position. The Co1–O$_{carboxylato}$ bond distance is the shortest one in the coordination sphere (1.967(2) Å) while the Co1–O$_{phenolato}$ and the Co1–N$_{neoc}$ bond distances are of similar lengths (2.051(2)–2.083(3) Å).

The cobalt(II) ions are bridged by two phenolato oxygen atoms forming a parallelogram (Co1–O3–Co1^i–O3^i) with sides of 2.051(2) and 1.997(2) Å and angles of 78.62(11)° and 100.56(10)°. The interatomic Co1⋯Co1^i separation distance is 3.114 Å and is in the range (2.923–3.4753 Å) found for two Co(II) bridged by two oxo-atoms.[88–92] The solvate methanol molecules are stabilised via the formation of hydrogen bonds (Table S6†).

3.2.3. Structure of complex 7. Complex 7 is the only complex in the current research that does not contain any nitrogen-donors as co-ligands. This is maybe the reason for the unsuccessful efforts to isolate single-crystals suitable for X-ray crystallography. However, the characterisation of complex 7 was based on all data collected (IR and UV-vis spectroscopy, and RT-magnetic measurements) which were compared with reported structures of similar Co(II)–NSAID complexes with O-donor co-ligands. Complex 7 is a mononuclear high-spin octahedral Co(II) compound based on the RT-magnetic data (μ_{eff} = 3.97 BM) and the UV-vis spectroscopic features. According to IR spectroscopy, the meclofenamato ligands are monodentately coordinated ($\Delta\nu(COO)$ = 191 cm^{-1}). Therefore, complex 7 is suggested to have a CoO$_6$ coordination sphere; two of the six oxygen atoms originate from the carboxylato groups of two meclofenamato ligands and the other four

oxygen atoms come from four methanol ligands (Fig. 4). Such arrangement is similar with that observed for complex **6b** and the cobalt(II) complexes with the NSAIDs Hmef, H$_2$difl and niflumic acid (= Hnif), i.e. [Co(mef)$_2$(MeOH)$_4$],[17] [Co(Hdifl)$_2$(MeOH)$_4$] and [Co(nif)$_2$(MeOH)$_4$],[43] respectively.

3.3. Antioxidant ability of the complexes

Free radicals are species with unpaired electron(s) and play a crucial role in inflammatory process. Radicals may transfer their unpaired electron(s) to adjacent molecule(s), and this process may ignite a series of chain reactions which are further responsible for diverse undesired side-effects in the organisms such as inflammations, swelling, or even cancer.[63] The anti-inflammatory activity and potential subsequent anticancer effects of NSAIDs and their compounds are often connected with their activity against free radicals; they can either inhibit or capture these radicals. As a result, compounds with antioxidant properties might play an important role towards inflammation and can be pioneers for developing effective pharmaceuticals.[93]

Within this context and taking into consideration the antioxidant efficacy of the free NSAIDs used as ligands in the complexes under study, the potential antioxidant activity of complexes **1–14** was evaluated through their ability to scavenge DPPH and ABTS radicals and to reduce H$_2$O$_2$. The results are summarised in Table S11† and depicted in Fig. 9, and were compared with the activity of well-known reference compounds NDGA, BHT, trolox and L-ascorbic acid (AA).[93,94]

The neutralisation of DPPH radicals by antioxidants gains continuous recognition due to its potential activity against cancer, aging process and/or inflammation. The DPPH radical is a stable free radical which exhibits an intense absorption band at λ_{max} = 517 nm.[50] The ability of the compounds to scavenge DPPH radicals was found to be mainly time-independent, as shown after measuring the absorbance after 30 min and 60 min reaction, except for complexes **1** and **7** whose
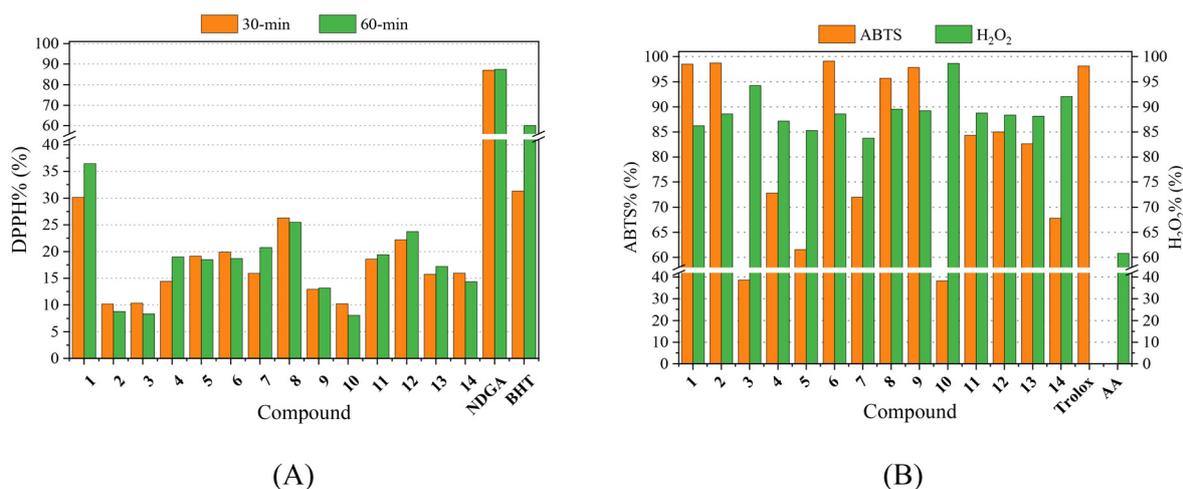
Fig. 9 (A) % DPPH-scavenging ability (DPPH%) for the compounds after 30-min and 60-min incubation. (B) % ABTS radical scavenging activity (ABTS%) and H$_2$O$_2$ reducing activity (H$_2$O$_2$%) for the compounds.

activity increased by ~5–6% upon time. Almost all complexes were more active towards DPPH than the corresponding free NSAIDs. However, when compared with the reference compounds NDGA and BHT, complexes **1–14** showed much lower DPPH-scavenging activity (Table S11,† Fig. 9). Among the complexes under study, $[Co(tolf)_2(Himi)_2]$ (complex **1**) exhibited the highest DPPH-scavenging activity (DPPH% = 30.18–36.44%) which was close to the short-term (30 min) activity of the reference compound BHT (31.30 ± 0.10%).

The overall antioxidant activity of compounds is related to their ability to scavenge the cationic ABTS radical (ABTS$^{•+}$). This process is based on the discoloration of a dark green solution containing the cationic radical ABTS$^{•+}$ resulting from the oxidation caused by a hydrogen-donating antioxidant agent.[51] In general, the activity of complexes **1–14** towards ABTS radicals is higher than the activity of the corresponding free NSAIDs (Fig. 9). When compared with the reference compound trolox, the activity of most complexes is moderate-to-high with complexes **1**, **2**, **6** and **9** being the most active compounds (ABTS% = 97.81–99.07%) approaching the ABTS-scavenging activity of trolox (= 98.10 ± 0.48%).

Hydrogen peroxide is an oxidizing agent capable to generate dangerous hydroxyl radicals ($^{•}OH$) when interacting with transition metal ions causing high oxidative stress. Therefore, scavengers of $^{•}OH$ or reductants of H_2O_2 may relieve oxidative stress and inhibit the production of reactive oxygen species.[95] The interaction of complexes **1–14** with H_2O_2 was studied revealing that all complexes are more active (H_2O_2% = 83.73–98.64%, Fig. 9) than the corresponding free NSAIDs and L-ascorbic acid (= 60.80 ± 0.20%) which is the reference compound.[96] Complex **10** ($[Co(nap)_2(neoc)]$) was the most active complex towards H_2O_2 (H_2O_2% = 98.64 ± 0.90%).

In total, all complexes **1–14** exhibited significant activity especially towards the ABTS radicals and hydrogen peroxide which is comparable with other metal–NSAIDs complexes.[16,17,37–39,41–43,47–49,51,54,55,63,97,98] When comparing the antioxidant activity of complexes **1–14** with that of the reported Co(II)–NSAID complexes,[16,17,41–43,73] we may conclude that complex **1** is among the top-three DPPH-scavengers (DPPH%: 42.42 ± 0.13% for $[Co(nap)_2(phen)(H_2O)_2]$;[16] 36.8% for $[Co(mef)_2(phen)(MeOH)_2]$;[17] 36.44 ± 0.11% for **1**), and complexes **1**, **2**, **6** and **9** are among the most active ABTS-scavengers (ABTS%: 99.07 ± 0.07% for **6**; 98.71 ± 0.14% for **2**; 98.48 ± 0.13% for **1**; 97.81 ± 0.06% for **9**; 96.7% for $[Co(mef)_2(py)_2(MeOH)_2]$[17]).

3.4. Interaction of the complexes with DNA

Coordination compounds can usually interact with DNA covalently (covalent binding to N atoms of DNA-bases) or noncovalently (via intercalation, electrostatically interactions, and/or major/minor groove binding) and/or may induce cleavage of the DNA-helix.[99,100] The interaction of herein reported complexes **1–14** with CT DNA (which is linear DNA) was studied by viscosity measurements, cyclic voltammetry, UV-vis spectroscopy, and via their ability to displace EB which was monitored by fluorescence emission spectroscopy. In addition, the interaction of the complexes with plasmid DNA (which is circular DNA) was studied via gel electrophoresis.

3.4.1. Affinity for CT DNA. The interaction of the corresponding free NSAIDs with CT DNA (viscosity measurements, UV-vis spectroscopy, and EB-displacing ability) has been previously reported[16,17,41,43,51,52] and the data are given in Tables 1 and 3 for comparison reasons. The UV-vis spectra of compounds **1–14** were recorded in the absence and presence of increasing amounts of CT DNA solution. The changes of the λ_{max} of the intra-ligand bands of the complexes were monitored to investigate the interaction with CT DNA and calculate the corresponding DNA-binding constants (K_b). One or two intra-ligand bands were observed in the UV-vis spectra of complexes **1–14** (representatively shown in Fig. S1†). Upon incremental addition of CT DNA solution, these bands I and II exhibited slight hyperchromism or hypochromism. In most cases, the changes in absorption were accompanied by a slight red-shift (Table 5) which may reveal a stabilisation of the novel complex–DNA adduct. The observed spectroscopic features reveal the interaction between the complexes and CT DNA, although their interaction mode cannot be safely concluded.[101] For this purpose, more specific experiments, including viscosity, cyclic voltammetry, and EB-displacement studies, were employed to elucidate the DNA-interaction mode of the compounds.

The Wolfe–Shimer equation (eqn (S1)†)[102] and the plots $[DNA]/(\varepsilon_A - \varepsilon_f)$ versus $[DNA]$ (Fig. S2†) were used for the calculation of the K_b values of the complexes. Almost all complexes **1–14** presented higher DNA-binding constants than the corresponding free NSAIDs (Table 1) with complex **6** being the tightest DNA-binder among the complexes according to its highest K_b

Table 1 UV-vis spectral features of complexes **1–14** with CT DNA. UV-band (λ in nm) (percentage of the observed hyper-/hypo-chromism ($\Delta A/A_0$, %), blue-/red-shift of the $\lambda_{max}(\Delta\lambda$, nm)) and DNA-binding constants (K_b)

Compound	λ (nm) ($\Delta A/A_0$ (%)[a], $\Delta\lambda$ (nm)[b])	K_b (M^{-1})
Complex 1	I: 301 (−4, 0)	9.79(±0.28) × 10^4
Complex 2	I: 300 (+3, +2), II: 334 (−10, 0)	3.58(±0.24) × 10^5
Complex 3	I: 320 (+2, +2), II: 332 (−1, 0)	3.51(±0.24) × 10^5
Complex 4	I: 297 (+12, +4), II: 317 (+8, +2)	3.15(±0.08) × 10^5
Complex 5	I: 300 (+10, +2), II: 317 (+5, 0)	1.14(±0.14) × 10^6
Complex 6	I: 291 (+4, +2)	1.62(±0.08) × 10^6
Complex 7	I: 299 (+10, +3), II: 321 (+1, 0)	3.16(±0.32) × 10^5
Complex 8	I: 296 (+2.5, +1)	4.80(±0.13) × 10^5
Complex 9	I: 311 (+20, +4), II: 348 (−40, elim[c])	4.14(±0.12) × 10^5
Complex 10	I: 318 (−15, +2), II: 333 (−4, +1)	6.55(±0.12) × 10^5
Complex 11	I: 292 (−6, −2), II: 316 (−4, 0)	4.60(±0.22) × 10^5
Complex 12	I: 289 (+1, −3), II: 328 (−11, 0)	3.18(±0.09) × 10^5
Complex 13	I: 296 (−4, +2), II: 318 (−8, 0)	1.01(±0.17) × 10^6
Complex 14	I: 296 (−4.5, 0), II: 319 (−12, 0)	4.59(±0.18) × 10^5
Htolf[41]	305 (+40, +5)	5.00(±0.10) × 10^4
Hmef[17]	324 (+10, 0)	1.05(±0.02) × 10^5
Hnap[16]	325 (+22, 0)	2.67(±0.22) × 10^4
Na meclf[51]	302 (−12, −1)	1.51(±0.12) × 10^5
Na dicl[52]	295 (−7.5, 0)	3.16(±0.14) × 10^4
H$_2$difl[43]	295 (+15, +2)	3.08(±0.15) × 10^3

[a] "+" denotes hyperchromism, "−" denotes hypochromism. [b] "+" denotes red-shift, "−" denotes blue-shift. [c] "elim" = eliminated.

value (= $1.62(\pm 0.08) \times 10^6$ M^{-1}). The K_b values of the complexes were also higher than that of the classic intercalator EB ($K_b = 1.23 \times 10^5$ M^{-1}).[103] The DNA-binding constants of all complexes were found in the range reported for similar Co(II)–NSAID complexes in the literature.[16,17,41–43,73] Comparing the DNA-binding constants of the Co(II)–NSAID complexes, complexes **5**, **6** and **13** are among the tightest DNA–binders bearing K_b values higher than 10^6 M^{-1} ($K_b = 1.01(\pm 0.17) \times 10^6$ M^{-1} for **13**; $1.14(\pm 0.14) \times 10^6$ M^{-1} for **5**; 1.14×10^6 M^{-1} for [Co(tolf)$_2$(MeOH)$_4$];[41] 1.62 $(\pm 0.08) \times 10^6$ M^{-1} for **6**; 2.28×10^6 M^{-1} for [Co(tolf)$_2$(phen) (MeOH)$_2$];[41] 3.03×10^6 M^{-1} for [Co$_2$(indo)$_4$(bipy)$_2$(H$_2$O)];[73] 3.57×10^6 M^{-1} for [Co$_3$(fluf)$_6$(bipy)$_2$] (Hfluf the NSAID flufenamic acid);[43] 9.41×10^6 M^{-1} for [Co(dicl)$_2$(bipy)];[42] 1.67×10^7 M^{-1} for [Co(dicl)$_2$(MeOH)$_4$][42]).

Cyclic voltammetry is used to acquire additional information for the DNA–interaction profile of coordination com-

pounds. In general, certain changes in the cyclic voltammograms of the complexes in the presence of CT DNA may shed light to the interaction mode between the coordination compounds and CT DNA. More specifically, the positive shift of a potential is evidence of intercalation, while a negative shift occurs in case of electrostatic interactions with DNA.[104]

The cyclic voltammograms of compounds **1–14** (0.33 mM) were recorded in the absence and presence of CT DNA solution (representatively shown for compounds **1** and **12** in Fig. 10). The cathodic potential (E_{pc}) and the anodic potential (E_{pa}) concerning the redox couple Co(II)/Co(I) for the complexes **1–14** and their shifts in presence of CT DNA are summarised in Table 2. The positive shifts of the potentials of the redox couple Co(II)/Co(I) for the complexes (up to +77 mV) may suggest an intercalating mode of interaction with CT DNA (Table 2). However, the presence of a negative shift is also
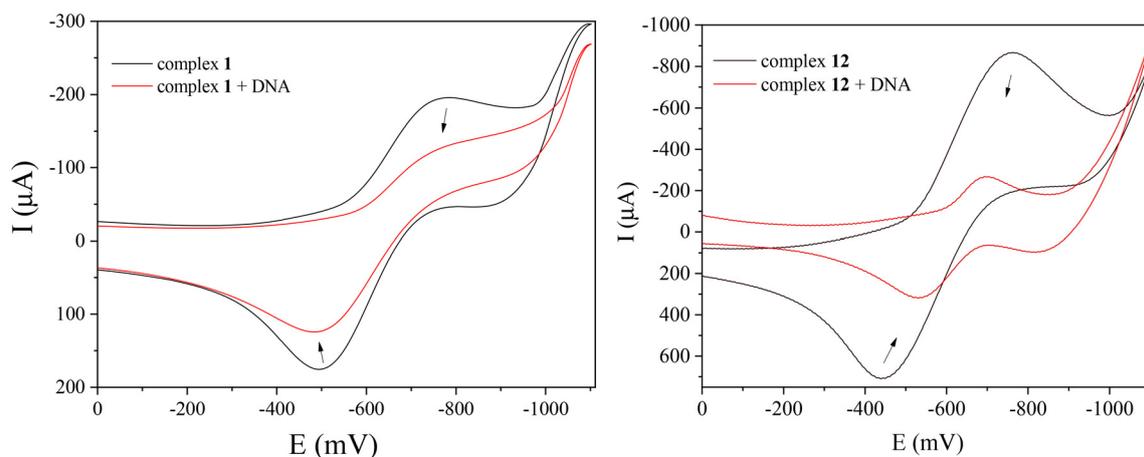
Fig. 10 Cyclic voltammograms of complexes **1** and **12** (0.33 mM, 1/2 DMSO/buffer), in the absence or presence of CT DNA. Scan rate = 100 mV s^{-1}. Supporting electrolyte = buffer solution. The arrows show the changes upon addition of CT DNA.

Table 2 Cathodic (E_{pc}) and anodic (E_{pa}) potentials (mV) for the redox couples Co(II)/Co(I) of complexes **1–14** in (0.33 mM) 1 : 2 DMSO : buffer solution in the absence ($E_{pc(f)}$, $E_{pa(f)}$) and presence ($E_{pc(b)}$, $E_{pa(b)}$) of CT DNA as well as their shifts (ΔE_{pc}, ΔE_{pa}). Ratio of equilibrium binding constants (K_r/K_{ox})

Complex	$E_{pc(f)}$[a]	$E_{pc(b)}$[b]	ΔE_{pc}[c]	$E_{pa(f)}$[d]	$E_{pa(b)}$[e]	ΔE_{pa}[f]	K_{red}/K_{ox}
Complex **1**	−780	−765	+15	−500	−480	+20	1.35
Complex **2**	−755	−700	+55	−440	−480	−40	1.14
Complex **3**	−714	−708	+6	−530	−520	+10	1.15
Complex **4**	−765	−700	+65	−475	−530	−55	1.09
Complex **5**	−770	−700	+70	−445	−495	−50	1.18
Complex **6**	−730	−715	+15	−503	−500	+3	1.17
Complex **7**	−785	−710	+75	−450	−495	−45	1.29
Complex **8**	−719	−699	+20	−415	−445	−30	0.92
Complex **9**	−740	−745	−5	−460	−450	+10	1.04
Complex **10**	−706	−711	−5	−537	−525	+12	1.06
Complex **11**	−721	−711	+10	−528	−514	+14	1.23
Complex **12**	−762	−700	+62	−440	−525	−85	0.83
Complex **13**	−777	−700	+77	−445	−520	−75	1.02
Complex **14**	−670	−675	−5	−492	−482	+10	1.04

[a] $E_{pc(f)} = E_{pc}$ in DMSO/buffer in the absence of CT DNA. [b] $E_{pc(b)} = E_{pc}$ in DMSO/buffer in the presence of CT DNA. [c] $\Delta E_{pc} = E_{pc(b)} − E_{pc(f)}$. [d] $E_{pa(f)} = E_{pa}$ in DMSO/buffer in the absence of CT DNA. [e] $E_{pa(b)} = E_{pc}$ in DMSO/buffer in the presence of CT DNA. [f] $\Delta E_{pa} = E_{pa(b)} − E_{pa(f)}$.

observed in some cases. In conclusion, these features cannot lead to safe conclusions about the interaction mode between the complexes and CT DNA, although the intercalation is the most possible interaction mode which may be accompanied by external interactions. The ratio of the DNA–binding constants for the reduced (K_{red}) and oxidised forms (K_{ox}) of the cobalt ions (K_{red}/K_{ox}) was calculated with eqn (S2)† [105] and is used to evaluate the redox equilibrium. For most complexes, the ratio K_{red}/K_{ox} is higher than 1 (Table 2) revealing that CT DNA may interact selectively with the reduced form of the complexes. [105]

The measurement of DNA-viscosity is usually employed to monitor the interaction mode between compounds and CT DNA. The viscosity of the DNA-solution is measured because it is sensitive to changes in the relative length of the DNA chain constituting viscometry a reliable method to clarify the DNA-interaction mode. The presence of a compound that binds externally to CT DNA (*i.e.* electrostatically or groove-binding) will probably induce a slight bending of the double DNA-helix, without significantly affecting its length (in some cases, a slight shortening may occur) and subsequently resulting in negligible changes (usually slight decrease) of the DNA-viscosity. A classic intercalation of the compound in-between DNA-bases will result in an increase in the length of the DNA helix because of the increase of the separation distance between DNA-base pairs in order to host the inserting compound, and subsequently the viscosity of CT DNA will exhibit an increase. [106] Furthermore, in the case of DNA-cleavage induced by the compound, the formation of much shorter fragments with significantly shorter relevant length will be revealed through a significant decrease of DNA-viscosity.

In the present study, the viscosity of a CT DNA solution (0.1 mM) was measured in the presence of incrementally increasing amounts of compounds **1–14** (up to r = [compound]/[DNA] = 0.35). For all compounds **1–14**, the viscosity increased (Fig. 11) suggesting intercalation as the most possible mode of their interaction with CT DNA. [107] In some cases, the lowering of DNA-viscosity at the early steps of incremental

addition of the compounds (r values up to 0.15) indicated an initial external interaction which aided to closer approach followed by intercalation.

Ethidium bromide is a typical DNA-intercalator since its planar phenanthridine ring inserts in-between two adjacent DNA-bases. As a fluorescent compound, EB exhibits an intense emission band at 592–594 nm when bound to CT DNA. For this reason, the changes of the fluorescence emission spectra of the EB–DNA adduct induced by the addition of a compound are monitored to investigate its potential interaction mode with CT DNA. The EB–DNA emission band at 592 nm will decrease upon addition of a compound which binds to CT DNA as strongly as or more strongly than EB does. A slight or negligible decrease in fluorescence emission indicates an inability to displace EB from the EB–DNA adduct and is usually observed for compounds that do not act as intercalators. [108]

In the current study, the fluorescence emission spectra of the EB–DNA adduct (which was formed after 1 h pretreatment of EB (40 μM) and CT DNA (40 μM) in buffer solution) were recorded in the presence of increasing amounts of solutions of complexes **1–14** and the occurring changes were monitored. The addition of the complexes in the EB–DNA solution led to a significant decrease in fluorescence emission band at 594 nm (Fig. 12). In total, the decrease of the intensity of the emission band attributed to the EB–DNA adduct was significant (up to 74.5% of the initial fluorescence, Table 3, Fig. S3†), and may be assigned to the displacement of EB from the EB–DNA adduct.

The ability of the compounds to induce quenching of the fluorescence emission EB–DNA band is evaluated through the value of the Stern–Volmer constants (K_{SV}) which were calculated with the Stern–Volmer equation (eqn (S3)†) and the corresponding Stern–Volmer plots (Fig. S4†). All complexes show relatively high K_{SV} values (Table 3), with complex **13** bearing the highest Stern–Volmer constant (K_{SV} = 5.68(±0.10) × 10^5 M^{-1}). In addition, the quenching constants (k_q) of the
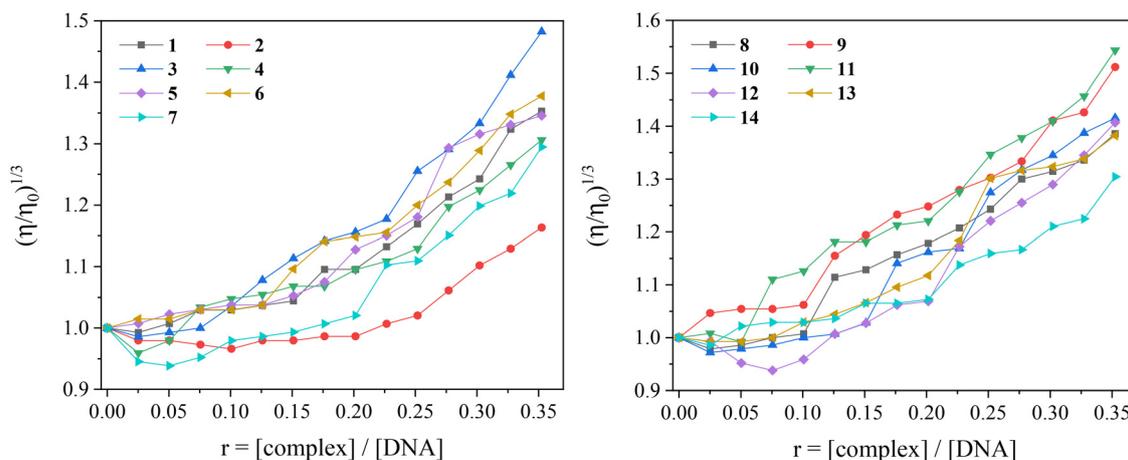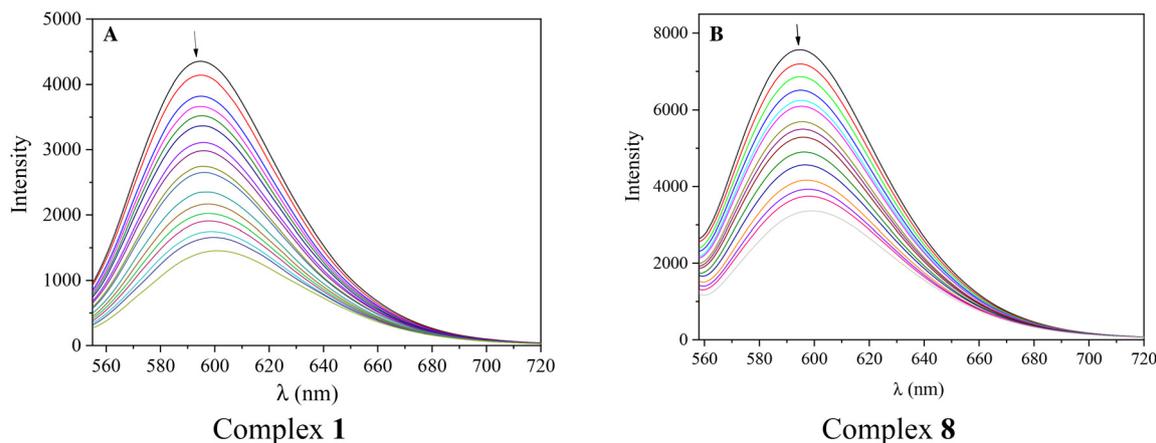

Fig. 11 Relative viscosity $(\eta/\eta_0)^{1/3}$ of CT DNA (0.1 mM) in buffer solution (150 mM NaCl and 15 mM trisodium citrate at pH 7.0) in the presence of complexes **1–14** at increasing amounts (r = [complex]/[DNA]).

Fig. 12 Fluorescence emission spectra ($\lambda_{excitation}$ = 540 nm) for EB–DNA conjugate ([EB] = 40 μM, [DNA] = 40 μM) in buffer solution (150 mM NaCl and 15 mM trisodium citrate at pH = 7.0) in the absence and presence of increasing amounts (up to r = [complex]/[DNA] = 0.21) of complex (A) **1** and (B) **8**. The arrows show the changes of intensity upon increasing amounts of the complexes.

Table 3 Fluorescence features of the EB-displacement studies of the NSAIDs and complexes **1–14**. Percentage of EB–DNA fluorescence emission quenching ($\Delta I/I_0$, in %), Stern–Volmer constants (K_{SV}, in M^{-1}) and quenching constants (k_q, in M^{-1} s^{-1})

Compound	$\Delta I/I_0$ (%)	K_{SV} (M^{-1})	k_q (M^{-1} s^{-1})
Complex 1	74.5	$3.50(\pm0.06) \times 10^5$	$1.52(\pm0.03) \times 10^{13}$
Complex 2	66.8	$1.89(\pm0.04) \times 10^5$	$8.21(\pm0.02) \times 10^{12}$
Complex 3	41.2	$2.71(\pm0.06) \times 10^4$	$1.18(\pm0.03) \times 10^{12}$
Complex 4	50.9	$1.01(\pm0.02) \times 10^5$	$4.39(\pm0.09) \times 10^{12}$
Complex 5	72.6	$2.04(\pm0.06) \times 10^5$	$8.87(\pm0.03) \times 10^{12}$
Complex 6	43.3	$1.09(\pm0.02) \times 10^5$	$4.75(\pm0.07) \times 10^{12}$
Complex 7	53.2	$1.08(\pm0.03) \times 10^5$	$4.68(\pm0.12) \times 10^{12}$
Complex 8	69.6	$4.55(\pm0.08) \times 10^5$	$1.98(\pm0.04) \times 10^{13}$
Complex 9	43.4	$5.50(\pm0.10) \times 10^4$	$2.39(\pm0.04) \times 10^{12}$
Complex 10	42.0	$3.52(\pm0.05) \times 10^4$	$1.53(\pm0.02) \times 10^{12}$
Complex 11	49.4	$1.01(\pm0.02) \times 10^5$	$4.38(\pm0.08) \times 10^{12}$
Complex 12	49.3	$9.87(\pm0.20) \times 10^4$	$4.29(\pm0.09) \times 10^{12}$
Complex 13	51.6	$5.68(\pm0.10) \times 10^5$	$2.47(\pm0.42) \times 10^{13}$
Complex 14	68.9	$5.42(\pm0.13) \times 10^5$	$2.36(\pm0.06) \times 10^{13}$
Htolf[41]	74.0	$1.15(\pm0.04) \times 10^6$	$5.00(\pm0.17) \times 10^{13}$
Hmef[17]	80.0	$1.58(\pm0.06) \times 10^5$	$6.87(\pm0.26) \times 10^{12}$
Hnap[16]	82.0	$1.47(\pm0.04) \times 10^5$	$6.39(\pm0.17) \times 10^{12}$
Na meclf[51]	80.1	$8.20(\pm0.26) \times 10^4$	$3.57(\pm0.11) \times 10^{12}$
Na dicl[52]	65.0	$2.47(\pm0.06) \times 10^5$	$1.07(\pm0.03) \times 10^{13}$
H_2difl[43]	65.0	$8.59(\pm0.35) \times 10^5$	$3.73(\pm0.15) \times 10^{13}$

complexes were calculated with eqn (S4)† (the value of fluorescence lifetime of EB–DNA system (τ_0) is equal to 23 ns[109]), and have significantly higher values (Table 3) than the value of 10^{10} M^{-1} s^{-1}, indicating a static quenching mechanism which may confirm the formation of a new adduct between CT DNA and each complex.

3.4.2. Cleavage of pBR322 plasmid DNA. In order to explore the ability of the complexes to act like nucleases, the cleavage of pBR322 plasmid DNA (pDNA) by the compounds was examined *via* agarose gel electrophoretic experiments. The supercoiled pDNA in an agarose gel during electrophoresis is shown as Form I (Fig. S5,† Lane 1). Complexes **1–13** (500 μM in DMSO solution, the amount of DMSO within the final

mixture never exceeded 10% v/v) were mixed with pDNA (25 μM, pH = 6.8, in tris buffer solution). After incubation for 30 min at 37 °C, the effect of the complexes on pDNA was analysed by gel electrophoresis on 1% agarose stained with EB (Fig. S5†).

The potential DNA-cleaving activity of complexes **1–13** (Fig. S5,† Lane 2–14) was revealed only as single-stranded (ss) nicks in the supercoiled DNA forming relaxed circular DNA (Form II), since no signal (double-stranded (ds) nick) attributed to the formation of linear DNA (Form III) was observed. The percentages of the cleavage (shown in Fig. S5†) were calculated with eqn (S5) and (S6).† At the high concentration of 500 μM used in the experiment, the compounds present low-to-negligible ability to cleave DNA with complex **8** being the only active among the compounds showing a 35% of cleavage (Fig. S5,† Lane 9). Although the reports concerning the pDNA-cleavage ability of metal–NSAID complexes are quite few,[110] it seems that herein reported Co(II)–NSAID complexes cannot induce significantly the cleavage of pDNA.

3.5. Interaction of the complexes with albumins

3.5.1. Affinity of the complexes for albumins. Serum albumin (SA) is probably the most predominant protein in bloodstream of mammals having various roles, mainly the maintenance of the osmotic pressure (it is essential for the maintenance of tissues) and the reversible binding of bioactive compounds (in order to transfer them towards their targets through the bloodstream).[111] Furthermore, the interaction with albumin may alter the biological properties of bioactive compounds and may reveal mechanistic pathways contributing to drug circulation and delivery. BSA is extensively studied because of its structural similarity with HSA, and possesses two tryptophan residues, Trp-134 and Trp-212, while HSA contains a single tryptophan at position 214.[108] Within this context, the interaction of complexes **1–14** with both albumins

HSA and BSA was investigated by fluorescence emission spectroscopy.

The interaction of complexes **1–14** with the albumins was studied by monitoring the quenching of tryptophan fluorescence emission band in the presence of incremental addition of the complexes. The fluorescence emission spectra of the albumins (3 mM) in buffer solution were recorded in the range 300–500 nm for $\lambda_{\text{excitation}} = 295$ nm (Fig. S6†). The incremental addition of complexes **1–14** resulted in a decrease of the intensity of the corresponding albumin emission band ($\lambda_{\text{max,emission}} = 340$ nm for HSA and 345 nm for BSA), while in the case of complex **14** an additional emission band (as previously reported for diflunisal and its complexes)[112] appeared at 415 nm (Fig. S6†). All complexes induced significant quenching of the albumin emission band which was more pronounced in the case of BSA than HSA (Fig. S7 and S8†). Such quenching may be attributed to re-arrangement of the SA secondary structure or its modifications as a result from the association with the complexes.[108] For the quantitative evaluation of this interaction, the fluorescence emission spectra (with $\lambda_{\text{excitation}} = 295$ nm) of the free complexes were subtracted from the overall spectra. The influence of the inner-filter effect on the measurements was assessed with eqn (S7),† [113] and was found negligible to affect the measurements.

The Stern–Volmer constant (K_{sv}), the SA-quenching constant (k_{q}) and the SA-binding constant (K) of the compounds were calculated with the Stern–Volmer and Scatchard equations (eqn (S3), (S4) and (S8)†) and plots (Fig. S9–S12†) considering that the fluorescence lifetime of tryptophan in SAs (τ_0) has the value of 10^{-8} s.[108] The calculated k_{q} values of complexes **1–14** are significantly higher (in most cases by two-to-three orders) than the value of 10^{10} M^{-1} s^{-1} (Table 4) and indicate that the quenching takes place *via* a static mechanism[108] which subsequently may confirm the interaction of the complexes with the albumins.

The values of the SA-binding constants of complexes **1–14** are of the 10^4–10^6 M^{-1} magnitude (Table 4) and fall within the range reported for many metal(II)–NSAID complexes.[16,17,37–43,47–49,51,54,55,63,97,98] Complexes **1** and **5** possess the highest K values for BSA among the compounds under study, while the highest HSA-binding constant was found for complex **5** (Table 4). Therefore, complex **5** is found to exhibit the highest affinity for both albumins among the herein studied complexes. A comparison with the albumin-binding constants of the reported Co(II)–NSAID complexes[16,17,41–43,73] may reveal that complexes **1–14** under study, especially complexes **1** and **5**, bear some of the highest BSA-binding constants ($>2 \times 10^6$ M^{-1}) among such complexes. The K values observed for complexes **1–14** are significantly lower than the value of the association constants of avidin with various compounds (*ca.* 10^{15} M^{-1}) which is considered the borderline for reversible noncovalent interactions. So, the SA-binding constants of the complexes suggest their reversible binding to the albumins, and the potential to be transferred by the albumins, and get released at their specific targets.[114]

3.5.2. Binding site of BSA. Each albumin contains four potential sites to encapsulate drugs and metal ions and the most critical sites are Sudlow's site 1 (or drug site I) and Sudlow's site 2 (or drug site II) in subdomains IIA and IIIA, respectively.[115] The potential albumin-binding site of a compound may be revealed by using the most common site-markers warfarin and ibuprofen, which bind selectively to drug sites I and II, respectively.[100,116] For this purpose, the BSA-binding constants of the complexes were calculated in the presence of warfarin and ibuprofen by fluorescence emission spectroscopy and compared with those found in the absence of any site-marker (values in Table 4).

The incremental addition of each complex in a solution containing BSA and the site-marker (warfarin or ibuprofen) resulted in a quenching of the initial fluorescence emission

Table 4 Albumin (BSA or HSA)-quenching constants (k_{q}, in M^{-1} s^{-1}) and albumin (BSA or HSA)-binding constants (K, in M^{-1}) of the compounds

Compound	$k_{\text{q(BSA)}}$ (M^{-1} s^{-1})	$K_{\text{(BSA)}}$ (M^{-1})	$k_{\text{q(HSA)}}$ (M^{-1} s^{-1})	$K_{\text{(HSA)}}$ (M^{-1})
Complex 1	$1.08(\pm0.06) \times 10^{14}$	$2.40(\pm0.29) \times 10^{6}$	$3.87(\pm0.14) \times 10^{12}$	$6.45(\pm0.20) \times 10^{4}$
Complex 2	$3.92(\pm0.29) \times 10^{13}$	$8.37(\pm0.10) \times 10^{5}$	$1.41(\pm0.07) \times 10^{12}$	$9.44(\pm0.30) \times 10^{4}$
Complex 3	$3.70(\pm0.11) \times 10^{12}$	$2.47(\pm0.07) \times 10^{5}$	$3.93(\pm0.17) \times 10^{11}$	$1.92(\pm0.07) \times 10^{4}$
Complex 4	$8.74(\pm0.44) \times 10^{13}$	$1.01(\pm0.04) \times 10^{6}$	$1.47(\pm0.07) \times 10^{12}$	$1.32(\pm0.07) \times 10^{5}$
Complex 5	$7.57(\pm0.52) \times 10^{13}$	$2.36(\pm0.11) \times 10^{6}$	$1.08(\pm0.04) \times 10^{12}$	$1.80(\pm0.08) \times 10^{5}$
Complex 6	$1.98(\pm0.08) \times 10^{13}$	$6.44(\pm0.19) \times 10^{5}$	$1.35(\pm0.04) \times 10^{12}$	$4.68(\pm0.16) \times 10^{4}$
Complex 7	$9.26(\pm0.58) \times 10^{13}$	$1.19(\pm0.04) \times 10^{6}$	$1.38(\pm0.08) \times 10^{12}$	$8.36(\pm0.39) \times 10^{4}$
Complex 8	$9.99(\pm0.42) \times 10^{13}$	$1.56(\pm0.37) \times 10^{6}$	$4.43(\pm0.17) \times 10^{12}$	$1.12(\pm0.37) \times 10^{5}$
Complex 9	$8.14(\pm0.21) \times 10^{13}$	$7.90(\pm0.24) \times 10^{5}$	$3.93(\pm0.10) \times 10^{12}$	$9.59(\pm0.50) \times 10^{4}$
Complex 10	$4.16(\pm0.17) \times 10^{12}$	$3.01(\pm0.14) \times 10^{4}$	$8.14(\pm0.31) \times 10^{11}$	$1.98(\pm0.06) \times 10^{4}$
Complex 11	$7.16(\pm0.40) \times 10^{13}$	$7.67(\pm0.38) \times 10^{5}$	$1.89(\pm0.08) \times 10^{12}$	$7.63(\pm0.31) \times 10^{4}$
Complex 12	$6.35(\pm0.39) \times 10^{13}$	$1.11(\pm0.05) \times 10^{6}$	$1.80(\pm0.04) \times 10^{12}$	$1.73(\pm0.07) \times 10^{4}$
Complex 13	$1.03(\pm0.05) \times 10^{14}$	$9.24(\pm0.51) \times 10^{5}$	$2.05(\pm0.10) \times 10^{12}$	$8.13(\pm0.41) \times 10^{4}$
Complex 14	$3.14(\pm0.20) \times 10^{13}$	$6.09(\pm0.15) \times 10^{5}$	$1.42(\pm0.05) \times 10^{12}$	$5.38(\pm0.21) \times 10^{4}$
Htolf[41]	$2.18(\pm0.12) \times 10^{13}$	$1.60(\pm0.14) \times 10^{5}$	$6.10(\pm0.38) \times 10^{12}$	$3.12(\pm0.25) \times 10^{5}$
Hmef[17]	$2.78(\pm0.20) \times 10^{13}$	$1.35(\pm0.22) \times 10^{5}$	$7.13(\pm0.34) \times 10^{12}$	$1.32(\pm0.15) \times 10^{5}$
Hnap[16]	$1.18(\pm0.06) \times 10^{12}$	$5.35(\pm0.42) \times 10^{3}$	$1.24(\pm0.09) \times 10^{12}$	$3.27(\pm0.30) \times 10^{4}$
Na meclf[51]	$4.84(\pm0.32) \times 10^{13}$	$1.78(\pm0.11) \times 10^{6}$	$2.98(\pm0.31) \times 10^{13}$	$1.05(\pm0.03) \times 10^{6}$
Na dicl[52]	$8.11(\pm0.34) \times 10^{12}$	$3.55(\pm0.03) \times 10^{5}$	$1.81(\pm0.17) \times 10^{12}$	1.63×10^{5}
H$_2$difl[43]	$1.53(\pm0.08) \times 10^{13}$	$1.93(\pm0.15) \times 10^{5}$	$2.67(\pm0.16) \times 10^{12}$	$1.22(\pm0.07) \times 10^{5}$
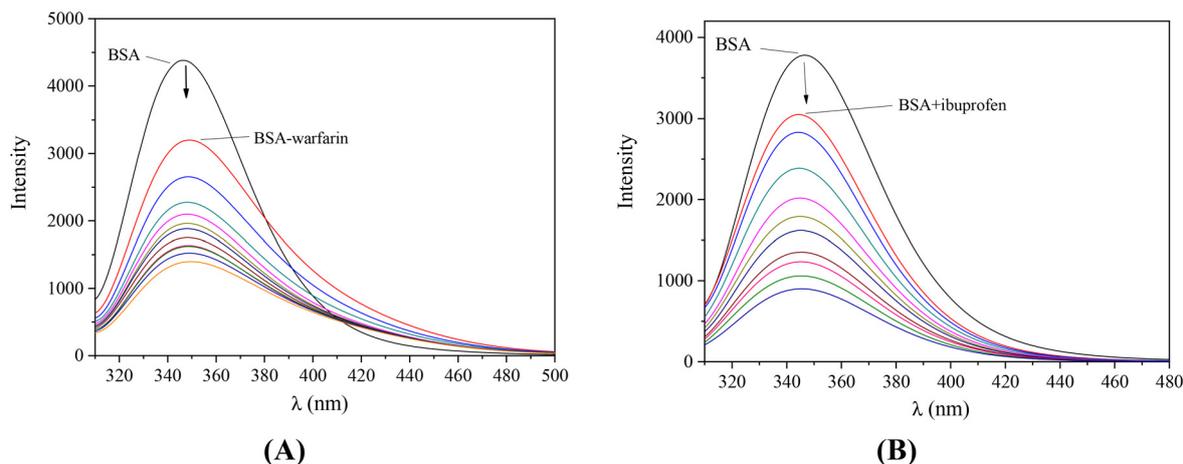
Fig. 13 Fluorescence emission spectra ($\lambda_{excitation}$ = 295 nm) of a buffer solution (150 mM NaCl and 15 mM trisodium citrate at pH 7.0) of BSA (3 μM) (A) in the presence of warfarin (3 μM) upon addition of increasing amounts of complex **1**, (B) in the presence of ibuprofen (3 μM) upon addition of increasing amounts of complex **2**. The arrows show the changes of intensity upon increasing amounts of the complexes.

band (representatively shown in Fig. 13). A decrease of the K value in presence of the site-marker indicates that the binding of the compound to albumin is influenced by the presence of this marker and can be attributed to the competition for the same binding site.[100,116] The SA-binding constants of the compounds in the presence of warfarin or ibuprofen were calculated (with the Scatchard equation (eqn (S8)†) and plots (Fig. S13 and S14†)) and their values (Table 5) are compared with those determined in the absence of any site-marker in order to check for the preferable drug site.

For almost all complexes (Table 5), a significant decrease of the BSA-binding constants in the presence of both warfarin and ibuprofen was found showing that the complexes may bind to Sudlow sites I and II, respectively. However, for complexes **1**, **2**, **5** and **10**, lower K values were calculated in the presence of ibuprofen than warfarin suggesting their preference for drug site II. On the other hand, for complexes **3**, **4**, **7**, **8**, and **11–12**, a selective binding to drug site I may be

suggested since the presence of warfarin led to lower K values than the presence of ibuprofen did.[100,116] For complexes **6**, **9**, **13** and **14**, the presence of both site-markers resulted in similarly decreased K values revealing the lack of selectivity for Sudlow sites I and II.

4. Conclusions

Fourteen cobalt(II) complexes with diverse carboxylate NSAIDs as ligands in the presence of a series of nitrogen-donors as co-ligands have been isolated and characterised. The crystal structures of eight out of the fourteen cobalt(II) complexes, *i.e.* complexes **1**, **2**, **5**, **6**, **8–10** and **14**, were determined by single-crystal X-ray crystallography. In complexes **1–13**, the NSAIDs are simply deprotonated acting as monodentate or bidentate chelating ligands. In complex **14**, diflunisal is doubly deprotonated and is bound as a tridentate bridging ligand leading to the formation of the dinuclear complex $[Co_2(difl)_2(neoc)_2] \cdot MeOH$. This is the first structure that diflunisal is coordinated in a tridentate bridging mode.

The *in vitro* potential biological profile of the complexes was evaluated regarding their interaction with biomacromolecules (albumins and DNA), and their antioxidant ability. The complexes may interact with CT DNA *via* intercalation and the highest DNA-binding constant was found for complex **6** (K_b = 1.62($\pm$0.08) $\times$ 10^6 M^{-1}). The ability of the complexes to cleave pBR322 plasmid DNA to relaxed circular DNA is rather low at the concentration of 500 μM, since only complex **8** showed noteworthy cleavage activity (up to 35%).

The binding of complexes **1–14** to bovine and human serum albumins is tight and reversible showing their potency for effective transportation towards potential biological targets of the complexes where they may get released in order to fulfil a possible biological mission. Furthermore, competitive studies with the typical site-markers warfarin and ibuprofen

Table 5 BSA-binding constants (in M^{-1}) of the complexes in the absence ($K_{(BSA)}$) or presence of the site-markers warfarin ($K_{(BSA,warf)}$) and ibuprofen ($K_{(BSA,ibu)}$)

Complex	$K_{(BSA)}$	$K_{(BSA,ibu)}$	$K_{(BSA,warf)}$
Complex 1	2.40($\pm$0.29) $\times$ 10^6	2.29($\pm$0.07) $\times$ 10^5	3.76($\pm$0.15) $\times$ 10^5
Complex 2	8.37($\pm$0.10) $\times$ 10^5	9.42($\pm$0.34) $\times$ 10^4	2.54($\pm$0.09) $\times$ 10^5
Complex 3	2.47($\pm$0.07) $\times$ 10^5	9.31($\pm$0.58) $\times$ 10^4	2.90($\pm$0.28) $\times$ 10^4
Complex 4	1.01($\pm$0.04) $\times$ 10^6	6.23($\pm$0.26) $\times$ 10^5	5.42($\pm$0.21) $\times$ 10^5
Complex 5	2.36($\pm$0.11) $\times$ 10^6	4.60($\pm$0.13) $\times$ 10^5	7.18($\pm$0.23) $\times$ 10^5
Complex 6	6.44($\pm$0.19) $\times$ 10^5	2.20($\pm$0.06) $\times$ 10^5	2.38($\pm$0.11) $\times$ 10^5
Complex 7	1.19($\pm$0.04) $\times$ 10^6	6.51($\pm$0.18) $\times$ 10^5	1.59($\pm$0.06) $\times$ 10^5
Complex 8	1.56($\pm$0.37) $\times$ 10^6	3.55($\pm$0.14) $\times$ 10^5	2.67($\pm$0.13) $\times$ 10^5
Complex 9	7.90($\pm$0.24) $\times$ 10^5	2.21($\pm$0.06) $\times$ 10^5	2.30($\pm$0.09) $\times$ 10^5
Complex 10	3.01($\pm$0.14) $\times$ 10^4	8.27($\pm$0.56) $\times$ 10^3	1.37($\pm$0.04) $\times$ 10^5
Complex 11	7.67($\pm$0.38) $\times$ 10^5	7.13($\pm$0.25) $\times$ 10^5	5.76($\pm$0.20) $\times$ 10^5
Complex 12	1.11($\pm$0.05) $\times$ 10^6	9.49($\pm$0.38) $\times$ 10^5	4.53($\pm$0.15) $\times$ 10^5
Complex 13	9.24($\pm$0.51) $\times$ 10^5	5.25($\pm$0.14) $\times$ 10^5	4.83($\pm$0.15) $\times$ 10^5
Complex 14	6.09($\pm$0.15) $\times$ 10^5	4.99($\pm$0.15) $\times$ 10^5	5.08($\pm$0.09) $\times$ 10^5

were employed to explore whether the complexes bind selectively to typical BSA-binding sites. A clear selectivity tendency was not revealed since almost equal numbers of the complexes prefer to bind at Sudlow's site 1 (in competition with warfarin) or Sudlow's site 2 (in competition with ibuprofen) or both sites (almost equal BSA-binding constants in the presence of warfarin and ibuprofen).

Regarding the antioxidant potency of the complexes, their ability to scavenge DPPH and ABTS free radicals and to reduce H_2O_2 was monitored. Almost all complexes were more active than the corresponding free NSAIDs. The DPPH-scavenging ability of the complexes is relatively low except for [Co(tolf)$_2$(Himi)$_2$] (complex **1**) which was the most active DPPH-scavenger with relatively moderate time-dependent activity (DPPH% = 30.18–36.44%). Most complexes showed significant ability to scavenge ABTS radicals with complexes **1**, **2**, **6** and **9** (ABTS% = 97.81–99.07%) being as active as the reference compound trolox. Concerning the activity towards H_2O_2, all complexes were found more active than the reference compound ʟ-ascorbic acid.

In conclusion, the cobalt(ɪɪ)–NSAID compounds showed significant ABTS scavenging and hydrogen peroxide reduction activity and may bind tightly to CT DNA. Such biological activity is a prerequisite for potential anticancer activity. Thus, the herein reported data combined with the affinity of the compounds for albumins may reveal a group of potentially bioactive compounds deserving further biological studies.

Abbreviations

AA	ʟ-Ascorbic acid
ABTS	2,2′-Azinobis-(3-ethylbenzothiazoline-6-sulfonic acid)
3-ampy	3-Aminopyridine
BHT	Butylated hydroxytoluene
bipy	2,2′-Bipyridine
bipyam	2,2′-Bipyridylamine
BSA	Bovine serum albumin
CT	Calf-thymus
dicl⁻	Anion of diclofenac
difl⁻²	Dianion of diflunisal
DPPH	1,1-Diphenyl-picrylhydrazyl
EB	Ethidium bromide
fluf⁻	Flufenamato anion
Hdicl	Diclofenac
Hdifl⁻	Anion of diflunisal
Hfluf	Flufenamic acid
Himi	1H-Imidazole
Hindo	Indomethacin
Hmeclf	Meclofenamic acid
Hmef	Mefenamic acid
Hnap	Naproxen
Hnif	Niflumic acid
HSA	Human serum albumin
Htolf	Tolfenamic acid
H₂difl	Diflunisal
indo⁻	Anion of indomethacin
K	SA-binding constant
K_b	DNA-binding constant
K_{ox}	DNA-binding constant for the oxidised form
k_q	Quenching constant
K_r	DNA-binding constant for the reduced form
K_{SV}	Stern–Volmer constant
meclf⁻	Meclofenamato anion
mef⁻	Mefenamato anion
nap⁻	Anion of naproxen
NDGA	Nordihydroguaiaretic acid
neoc	Neocuproine, 2,9-dimethyl-1,10-phenanthroline
nif⁻	Niflumato anion
NSAID	Non-steroidal anti-inflammatory drugs
RT	Room-temperature
phen	1,10-Phenanthroline
py	Pyridine
SA	Serum albumin
trolox	6-Hydroxy-2,5,7,8-tetramethylchromane-2-carboxylic acid
tolf⁻	Tolfenamato anion
$\Delta\nu(COO)$	$\nu_{asym}(COO) - \nu_{sym}(COO)$

Data availability

The data supporting this article have been included as part of the ESI.†

CCDC deposition numbers 2336775–2336782 contain the supplementary crystallographic data for the complexes. Supplementary data associated with this article can be found in the online version, at https://doi.org/10.1039/d4dt01846j.

Conflicts of interest

There are no conflicts to declare.

References

1 P. Chellan and P. J. Sadler, *Philos. Trans. R. Soc., A*, 2015, **373**, 2014018.
2 M. A. Zoroddu, J. Aaseth, G. Crisponi, S. Medici, M. Peana and V. M. Nurchi, *J. Inorg. Biochem.*, 2019, **195**, 120–129.
3 K. Yamada, *Met. Ions Life Sci.*, 2013, **13**, 295–320.
4 P. J. Sadler, *Adv. Inorg. Chem.*, 1991, **36**, 1–48.
5 Y. gui Gao, M. Sriram and A. H. J. Wang, *Nucleic Acids Res.*, 1993, **21**, 4093–4101.
6 E. L. Baldwin, J. A. W. Byl and N. Osheroff, *Biochemistry*, 2004, **43**, 728–735.
7 M. C. Heffern, N. Yamamoto, R. J. Holbrook, A. L. Eckermann and T. J. Meade, *Curr. Opin. Chem. Biol.*, 2013, **17**, 189–196.

8 A. K. Renfrew, E. S. O'Neill, T. W. Hambley and E. J. New, *Coord. Chem. Rev.*, 2018, **375**, 221–233.

9 Z. Zhao, J. Zhang, S. Zhi, W. Song and J. Zhao, *J. Inorg. Biochem.*, 2019, **197**, 110696.

10 H. Crlikova, H. Kostrhunova, J. Pracharova, M. Kozsup, S. Nagy, P. Buglyó, V. Brabec and J. Kasparkova, *JBIC, J. Biol. Inorg. Chem.*, 2020, **25**, 339–350.

11 L. Q. Chai, L. Zhou, H. Bin Zhang, K. H. Mao and H. S. Zhang, *New J. Chem.*, 2019, **43**, 12417–12430.

12 G. Balan, O. Burduniuc, I. Usataia, V. Graur, Y. Chumakov, P. Petrenko, V. Gudumac, A. Gulea and E. Pahontu, *Appl. Organomet. Chem.*, 2020, **34**, e5423.

13 A. M. Mansour and M. S. Ragab, *RSC Adv.*, 2019, **9**, 30879–30887.

14 A. P. King, H. A. Gellineau, S. N. Macmillan and J. J. Wilson, *Dalton Trans.*, 2019, **48**, 5987–6002.

15 E. L. Chang, C. Simmers and D. A. Knight, *Pharmaceuticals*, 2010, **3**, 1711–1728.

16 F. Dimiza, A. N. Papadopoulos, V. Tangoulis, V. Psycharis, C. P. Raptopoulou, D. P. Kessissoglou and G. Psomas, *J. Inorg. Biochem.*, 2012, **107**, 54–64.

17 F. Dimiza, A. N. Papadopoulos, V. Tangoulis, V. Psycharis, C. P. Raptopoulou, D. P. Kessissoglou and G. Psomas, *Dalton Trans.*, 2010, **39**, 4517–4528.

18 C. N. Banti and S. K. Hadjikakou, *Eur. J. Inorg. Chem.*, 2016, 3048–3071.

19 G. Psomas and D. P. Kessissoglou, *Dalton Trans.*, 2013, **42**, 6252–6276.

20 A. R. Amin, P. Vyas, M. Attur, J. Leszczynska-Piziak, I. R. Patel, G. Weissmann and S. B. Abramson, *Proc. Natl. Acad. Sci. U. S. A.*, 1995, **92**, 7926–7930.

21 K. S. Kim, J. H. Yoon, J. K. Kim, S. J. Baek, T. E. Eling, W. J. Lee, J. H. Ryu, J. G. Lee, J. H. Lee and J. B. Yoo, *Biochem. Biophys. Res. Commun.*, 2004, **325**, 1298–1303.

22 A. Inoue, S. Muranaka, H. Fujita, T. Kanno, H. Tamai and K. Utsumi, *Free Radicals Biol. Med.*, 2004, **37**, 1290–1299.

23 D. Ho Woo, I. S. Han and G. Jung, *Life Sci.*, 2004, **75**, 2439–2449.

24 T. Pringsheim, W. J. Davenport and D. Dodick, *Neurology*, 2008, **70**, 1555–1563.

25 E. Moilanen and H. Kankaanranta, *Pharmacol. Toxicol.*, 1994, **75**, 60–63.

26 A. S. Kalgutkar, B. C. Crews, S. W. Rowlinson, A. B. Marnett, K. R. Kozak, R. P. Remmel and L. J. Marnett, *Proc. Natl. Acad. Sci. U. S. A.*, 2000, **97**, 925–930.

27 L. French, *Am. Fam. Physician*, 2005, **71**, 285–291.

28 F. Ruschitzka, J. S. Borer, H. Krum, A. J. Flammer, N. D. Yeomans, P. Libby, T. F. Lüscher, D. H. Solomon, M. E. Husni, D. Y. Graham, D. A. Davey, L. M. Wisniewski, V. Menon, R. Fayyad, B. Beckerman, D. Iorga, A. M. Lincoff and S. E. Nissen, *Eur. Heart J.*, 2017, **38**, 3282–3292.

29 S. E. Nissen, N. D. Yeomans, D. H. Solomon, T. F. Lüscher, P. Libby, M. E. Husni, D. Y. Graham, J. S. Borer, L. M. Wisniewski, K. E. Wolski, Q. Wang, V. Menon, F. Ruschitzka, M. Gaffney, B. Beckerman, M. F. Berger, W. Bao and A. M. Lincoff, *N. Engl. J. Med.*, 2016, **375**, 2519–2529.

30 W. J. Wechter, E. D. Murray, D. Kantoci, D. D. Quiggle, D. D. Leipold, K. M. Gibson and J. D. McCracken, *Life Sci.*, 2000, **66**, 745–753.

31 G. M. Lawton and P. J. Chapman, *Aust. Dent. J.*, 1993, **38**, 265–271.

32 G. Lohrmann, A. Pipilas, R. Mussinelli, D. M. Gopal, J. L. Berk, L. H. Connors, N. Vellanki, J. Hellawell, O. K. Siddiqi, J. Fox, M. S. Maurer and F. L. Ruberg, *J. Card. Failure*, 2020, **26**, 753–759.

33 D. Wojcieszyńska, H. Guzik and U. Guzik, *Sci. Total Environ.*, 2022, **834**, 155317.

34 M. T. Kelleni, *Biomed. Pharmacother.*, 2021, **133**, 110982.

35 G. D. Geromichalos, A. Tarushi, K. Lafazanis, A. A. Pantazaki, D. P. Kessissoglou and G. Psomas, *J. Inorg. Biochem.*, 2018, **187**, 41–55.

36 A. Tarushi, G. D. Geromichalos, D. P. Kessissoglou and G. Psomas, *J. Inorg. Biochem.*, 2019, **190**, 1–14.

37 M. Zampakou, N. Rizeq, V. Tangoulis, A. N. Papadopoulos, F. Perdih, I. Turel and G. Psomas, *Inorg. Chem.*, 2014, **53**, 2040–2052.

38 F. Dimiza, C. P. Raptopoulou, V. Psycharis, A. N. Papadopoulos and G. Psomas, *New J. Chem.*, 2018, **42**, 16666–16681.

39 F. Dimiza, A. G. Hatzidimitriou, Y. Sanakis, A. N. Papadopoulos and G. Psomas, *J. Inorg. Biochem.*, 2021, **218**, 111410.

40 F. Dimiza, A. Barmpa, A. Chronakis, A. G. Hatzidimitriou, Y. Sanakis, A. N. Papadopoulos and G. Psomas, *Int. J. Mol. Sci.*, 2023, **24**, 6391.

41 S. Tsiliou, L. A. Kefala, F. Perdih, I. Turel, D. P. Kessissoglou and G. Psomas, *Eur. J. Med. Chem.*, 2012, **48**, 132–142.

42 S. Perontsis, A. Dimitriou, P. Fotiadou, A. G. Hatzidimitriou, A. N. Papadopoulos and G. Psomas, *J. Inorg. Biochem.*, 2019, **196**, 110688.

43 S. Tsiliou, L. A. Kefala, A. G. Hatzidimitriou, D. P. Kessissoglou, F. Perdih, A. N. Papadopoulos, I. Turel and G. Psomas, *J. Inorg. Biochem.*, 2016, **160**, 125–139.

44 R. Smolkova, V. Zelenak, L. Smolko and M. Dusek, *Z. Kristallogr. - Cryst. Mater.*, 2016, **231**, 715–724.

45 R. Smolkova, L. Smolko, E. Samolova and M. Dusek, *J. Mol. Struct.*, 2023, **1272**, 134172.

46 G. G. Nnabuike, S. Salunke-Gawali, A. S. Patil, R. J. Butcher, J. A. Obaleye, H. Ashtekar and B. Prakash, *J. Mol. Struct.*, 2023, **1285**, 135519.

47 S. Perontsis, A. G. Hatzidimitriou, A. N. Papadopoulos and G. Psomas, *J. Inorg. Biochem.*, 2016, **162**, 9–21.

48 A. Barmpa, G. D. Geromichalos, A. G. Hatzidimitriou and G. Psomas, *J. Inorg. Biochem.*, 2021, **222**, 111507.

49 X. Totta, A. A. Papadopoulou, A. G. Hatzidimitriou, A. Papadopoulos and G. Psomas, *J. Inorg. Biochem.*, 2015, **145**, 79–93.

50 F. Dimiza, S. Fountoulaki, A. N. Papadopoulos, C. A. Kontogiorgis, V. Tangoulis, C. P. Raptopoulou, V. Psycharis, A. Terzis, D. P. Kessissoglou and G. Psomas, *Dalton Trans.*, 2011, **40**, 8555–8568.

51 A. Barmpa, A. G. Hatzidimitriou and G. Psomas, *J. Inorg. Biochem.*, 2021, **217**, 111357.

52 F. Dimiza, F. Perdih, V. Tangoulis, I. Turel, D. P. Kessissoglou and G. Psomas, *J. Inorg. Biochem.*, 2011, **105**, 476–489.

53 G. Malis, A. S. Bakali, A. G. Hatzidimitriou and G. Psomas, *J. Mol. Struct.*, 2024, **1303**, 137590.

54 A. Tarushi, X. Totta, A. Papadopoulos, J. Kljun, I. Turel, D. P. Kessissoglou and G. Psomas, *Eur. J. Med. Chem.*, 2014, **74**, 187–198.

55 A. Tarushi, Z. Karaflou, J. Kljun, I. Turel, G. Psomas, A. N. Papadopoulos and D. P. Kessissoglou, *J. Inorg. Biochem.*, 2013, **128**, 85–96.

56 A. Tarushi, C. Kakoulidou, C. P. Raptopoulou, V. Psycharis, D. P. Kessissoglou, I. Zoi, A. N. Papadopoulos and G. Psomas, *J. Inorg. Biochem.*, 2017, **170**, 85–97.

57 C. N. Banti, A. G. Hatzidimitriou, N. Kourkoumelis and S. K. Hadjikakou, *J. Inorg. Biochem.*, 2019, **194**, 7–18.

58 S. Caglar, A. Altay, B. Harurluoglu, E. K. K. Yeniceri, B. Caglar and O. Şahin, *J. Coord. Chem.*, 2022, **75**, 178–196.

59 Y. T. Wang, G. M. Tang, W. Z. Wan, Y. Wu, T. C. Tian, J. H. Wang, C. He, X. F. Long, J. J. Wang and S. W. Ng, *CrystEngComm*, 2012, **14**, 3802–3812.

60 C. N. Banti, E. I. Gkaniatsou, N. Kourkoumelis, M. J. Manos, A. J. Tasiopoulos, T. Bakas and S. K. Hadjikakou, *Inorg. Chim. Acta*, 2014, **423**, 98–106.

61 A. Johnson, C. Olelewe, J. H. Kim, J. Northcote-Smith, R. T. Mertens, G. Passeri, K. Singh, S. G. Awuah and K. Suntharalingam, *Chem. Sci.*, 2023, **14**, 557–565.

62 Y. L. Li, Q. Y. Liu, C. M. Liu, Y. L. Wang and L. Chen, *Aust. J. Chem.*, 2014, **68**, 488–492.

63 G. Psomas, *Coord. Chem. Rev.*, 2020, **412**, 213259.

64 J. Marmur, *J. Mol. Biol.*, 1961, **3**, 208–218.

65 M. E. Reichmann, S. A. Rice, C. A. Thomas and P. Doty, *J. Am. Chem. Soc.*, 1954, **76**, 3047–3053.

66 *Bruker Analytical X-ray Systems, Inc. Apex2, Version 2 User Manual, M86-E01078*, 2006.

67 *Siemens Industrial Automation, Inc. SADABS: Area-Detector Absorption Correction*, 1996.

68 L. Palatinus and G. Chapuis, *J. Appl. Crystallogr.*, 2007, **40**, 786–790.

69 P. W. Betteridge, J. R. Carruthers, R. I. Cooper, K. Prout and D. J. Watkin, *J. Appl. Crystallogr.*, 2003, **36**, 1487–1487.

70 W. J. Geary, *Coord. Chem. Rev.*, 1971, **7**, 81–122.

71 P. V. Bernhardt and G. A. Lawrance, *Compr. Coord. Chem. II*, 2003, **6**, 1–145.

72 K. Nakamoto, *Infrared and Raman Spectra of Inorganic and Coordination Compounds: Part B: Applications in Coordination, Organometallic, and Bioinorganic Chemistry*, 2008, pp. 1–408.

73 S. Perontsis, E. Geromichalou, F. Perdih, A. G. Hatzidimitriou, G. D. Geromichalos, I. Turel and G. Psomas, *J. Inorg. Biochem.*, 2020, **212**, 111213.

74 L. P. Battaglia, A. B. Corradi, G. Marcotrigiano, L. Menabue and G. C. Pellacani, *Inorg. Chem.*, 1979, **18**, 148–152.

75 L. Yang, D. R. Powell and R. P. Houser, *Dalton Trans.*, 2007, 955–964.

76 A. Okuniewski, D. Rosiak, J. Chojnacki and B. Becker, *Polyhedron*, 2015, **90**, 47–57.

77 B. Chakraborty and T. K. Paine, *Inorg. Chim. Acta*, 2011, **378**, 231–238.

78 M. L. Kirk, W. E. Hatfield, M. S. Lah, D. P. Kessissoglou, V. L. Pecoraro and C. Raptopoulou, *Inorg. Chem.*, 1991, **30**, 3900–3907.

79 S. Taktak, M. Flook, B. M. Foxman, L. Que and E. V. Rybak-Akimova, *Chem. Commun.*, 2005, 5301–5303.

80 J. A. van der Horn, B. Souvignier and M. Lutz, *Crystals*, 2017, **7**, 377.

81 Y. Wang and N. Okabe, *Acta Crystallogr., Sect. E: Struct. Rep. Online*, 2004, **60**, m1434–m1436.

82 Y. Yang, P. Du, J. F. Ma, W. Q. Kan, B. Liu and J. Yang, *Cryst. Growth Des.*, 2011, **11**, 5540–5553.

83 S. K. Langley, N. F. Chilton, B. Moubaraki and K. S. Murray, *Dalton Trans.*, 2011, **40**, 12201–12209.

84 Z. Xiao, G. Passeri, J. Northcote-Smith, K. Singh and K. Suntharalingam, *Chem. – Eur. J.*, 2021, **27**, 13846–13854.

85 L. Kuckova, K. Jomova, A. Svorcova, M. Valko, P. Segla, J. Moncol and J. Kozísek, *Molecules*, 2015, **20**, 2115–2137.

86 N. Palanisami, G. Prabusankar and R. Murugavel, *Inorg. Chem. Commun.*, 2006, **9**, 1002–1006.

87 A. W. Addison, T. N. Rao, J. Reedijk, J. Van Rijn and G. C. Verschoor, *J. Chem. Soc., Dalton Trans.*, 1984, 1349–1356.

88 M. J. Murphy, P. M. Usov, F. J. Rizzuto, C. J. Kepert and D. M. D'Alessandro, *New J. Chem.*, 2014, **38**, 5856–5860.

89 I. A. Koval, M. Huisman, A. F. Stassen, P. Gamez, M. Lutz, A. L. Spek, D. Pursche, B. Krebs and J. Reedijk, *Inorg. Chim. Acta*, 2004, **357**, 294–300.

90 L. N. Saunders, M. E. Pratt, S. E. Hann, L. N. Dawe, A. Decken, F. M. Kerton and C. M. Kozak, *Polyhedron*, 2012, **46**, 53–65.

91 S. Kita, H. Furutachi and H. Okawa, *Inorg. Chem.*, 1999, **38**, 4038–4045.

92 X. Meng, H. Hou, G. Li, B. Ye, T. Ge, Y. Fan, Y. Zhu and H. Sakiyama, *J. Organomet. Chem.*, 2004, **689**, 1218–1229.

93 C. Kontogiorgis, M. Ntella, L. Mpompou, F. Karallaki, P. Athanasios, D. Hadjipavlou-Litina and D. Lazari, *J. Enzyme Inhib. Med. Chem.*, 2016, **31**, 154–159.

94 S. Dairi, M. A. Carbonneau, T. Galeano-Diaz, H. Remini, F. Dahmoune, O. Aoun, A. Belbahi, C. Lauret, J. P. Cristol and K. Madani, *Food Chem.*, 2017, **237**, 297–304.

95 M. Wettasinghe and F. Shahidi, *Food Chem.*, 2000, **70**, 17–26.

96 B. M. Ali, M. Boothapandi and A. S. Sultan Nasar, *Data Brief*, 2020, **28**, 104972.

97 X. Totta, A. G. Hatzidimitriou, A. N. Papadopoulos and G. Psomas, *New J. Chem.*, 2017, **41**, 4478–4492.

98 M. Lazou, A. G. Hatzidimitriou, A. N. Papadopoulos and G. Psomas, *J. Inorg. Biochem.*, 2023, **243**, 112196.

99 B. J. Pages, D. L. Ang, E. P. Wright and J. R. Aldrich-Wright, *Dalton Trans.*, 2015, **44**, 3505–3526.

100 C. Kakoulidou, P. S. Gritzapis, A. G. Hatzidimitriou, K. C. Fylaktakidou and G. Psomas, *J. Inorg. Biochem.*, 2020, **211**, 111194.

101 A. M. Pyle, J. P. Rehmann, R. Meshoyrer, C. V. Kumar, N. J. Turro and J. K. Barton, *J. Am. Chem. Soc.*, 2002, **111**, 3051–3058.

102 A. Wolfe, G. H. Shimer and T. Meehan, *Biochemistry*, 1987, **26**, 6392–6396.

103 A. Dimitrakopoulou, C. Dendrinou-Samara, A. A. Pantazaki, M. Alexiou, E. Nordlander and D. P. Kessissoglou, *J. Inorg. Biochem.*, 2008, **102**, 618–628.

104 P. Zivec, F. Perdih, I. Turel, G. Giester and G. Psomas, *J. Inorg. Biochem.*, 2012, **117**, 35–47.

105 M. T. Carter, M. Rodriguez and A. J. Bard, *J. Am. Chem. Soc.*, 1989, **111**, 8901–8911.

106 J. L. Garcia-Gimenez, M. Gonzalez-Alvarez, M. Liu-Gonzalez, B. Macías, J. Borras and G. Alzuet, *J. Inorg. Biochem.*, 2009, **103**, 923–934.

107 A. M. Pizarro and P. J. Sadler, *Biochimie*, 2009, **91**, 1198–1211.

108 J. R. Lakowicz, *Principles of fluorescence spectroscopy*, Springer, 2006.

109 D. P. Heller and C. L. Greenstock, *Biophys. Chem.*, 1994, **50**, 305–312.

110 S. Perontsis, C. T. Chasapis, A. G. Hatzidimitriou and G. Psomas, *J. Inorg. Biochem.*, 2021, **223**, 111534.

111 R. E. Olson and D. D. Christ, *Annu. Rep. Med. Chem.*, 1996, **31**, 327–336.

112 S. Fountoulaki, F. Perdih, I. Turel, D. P. Kessissoglou and G. Psomas, *J. Inorg. Biochem.*, 2011, **105**, 1645–1655.

113 L. Stella, A. L. Capodilupo and M. Bietti, *Chem. Commun.*, 2008, 4744–4746.

114 O. H. Laitinen, V. P. Hytönen, H. R. Nordlund and M. S. Kulomaa, *Cell. Mol. Life Sci.*, 2006, **63**, 2992–3017.

115 G. Sudlow, D. J. Birkett and D. N. Wade, *Mol. Pharmacol.*, 1976, **12**, 1052–1061.

116 M. Lazou, A. Tarushi, P. Gritzapis and G. Psomas, *J. Inorg. Biochem.*, 2020, **206**, 111019.